ChemPhysChem

Review
doi.org/10.1002/cphc.202300806

Chemistry Europe
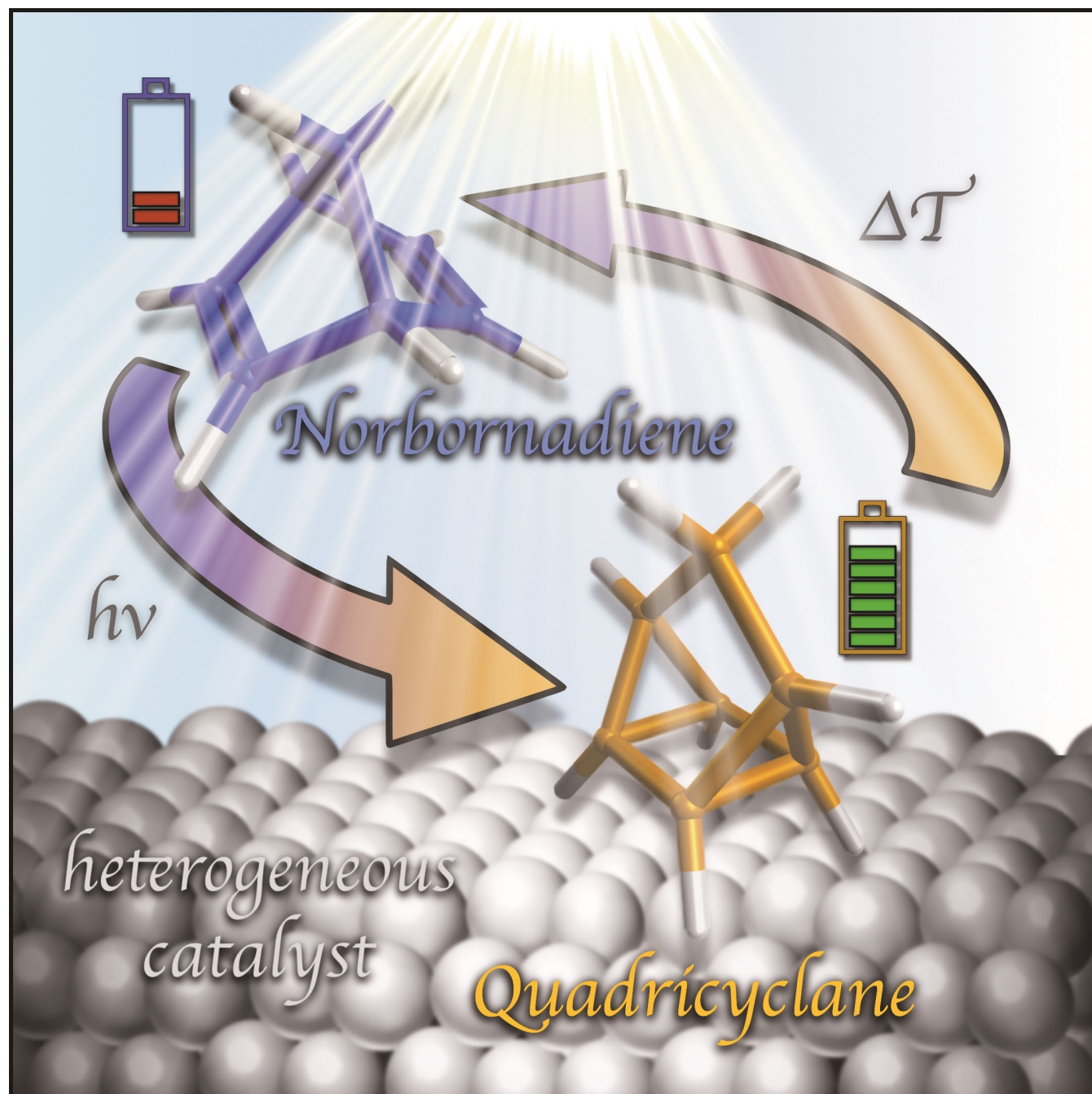European Chemical
Societies Publishing

www.chemphyschem.org

The Norbornadiene/Quadricyclane Pair as Molecular Solar Thermal Energy Storage System: Surface Science Investigations

Felix Hemauer,[a, b] Hans-Peter Steinrück,[a, c] and Christian Papp*[b, c]

ChemPhysChem

Review
doi.org/10.1002/cphc.202300806

Chemistry Europe
European Chemical
Societies Publishing

For the transition to renewable energy sources, novel energy storage materials are more important than ever. This review addresses so-called molecular solar thermal (MOST) systems, which appear very promising since they combine light harvesting and energy storing in one-photon one-molecule processes. The focus is on norbornadiene (NBD), a particularly interesting candidate, which is converted to the strained valence isomer quadricyclane (QC) upon irradiation. The stored energy can be released on demand. The energy-releasing cycloreversion from QC to NBD can be initiated by a thermal, catalytic, or electrochemical trigger. The reversibility of the energy storage and release cycles determines the general practicality of a MOST system. In the search for derivatives, which enable large-scale applications, fundamental surface science studies help to assess the feasibility of potential substituted NBD/QC couples. We include investigations under well-defined ultra-high vacuum (UHV) conditions as well as experiments in liquid phase. Next to the influence of the catalytically active surfaces on the isomerization between the two valence isomers, information on adsorption geometries, thermal stability limits, and reaction pathways of the respective molecules are discussed. Moreover, laboratory-scaled test devices demonstrate the proof of concept in various areas of application.

1. Introduction

1.1. Molecular Solar Thermal (MOST) Systems

The primary energy demand is expected to increase by about 1% per year up to 2030 reaching 485 EJ for the world consumption in the Stated Policies Scenario.[1] However, the need to reduce climate-damaging emissions[2] urges the transition from fossil to renewable energy sources.[3] To master these two diverging developments, novel energy storage solutions are indispensable. In this way, seasonal and regional fluctuations of solar and wind power, due to their intermittent character, can be counteracted, and the mismatch between load and supply during the course of a day can be compensated.[4]

Next to improvements in battery technologies,[5] there are different approaches for storing energy in a chemical manner. So-called molecular solar thermal (MOST) systems[6] combine the light-harvesting process with storage of the gained energy in a single step. Upon irradiation, an energy-lean parent compound is converted into its energy-rich valence isomer. In the latter, the energy difference between the two photoisomers is stored as intrinsic strain in the molecular framework, that is, the metastable state acts as storage unit. On demand, the stored energy can be released by triggering the back reaction, which occurs in a thermal, catalytic, or electrochemical manner. Thereby, the temporal and spatial solar power production and storage is decoupled from its energy consumption.

[a] F. Hemauer, Prof. Dr. H.-P. Steinrück
Lehrstuhl für Physikalische Chemie II, Friedrich-Alexander-Universität Erlangen-Nürnberg, Egerlandstr. 3, 91058 Erlangen, Germany

[b] F. Hemauer, Prof. Dr. C. Papp
Angewandte Physikalische Chemie, Freie Universität Berlin, Arnimallee 22, 14195 Berlin, Germany
E-mail: christian.papp@fu-berlin.de

[c] Prof. Dr. H.-P. Steinrück, Prof. Dr. C. Papp
Erlangen Center for Interface Research and Catalysis (ECRC), Friedrich-Alexander-Universität Erlangen-Nürnberg, Egerlandstr. 3, 91058 Erlangen, Germany

Several criteria of the respective energy storage systems have to be fulfilled for a reasonable application.[7] Most apparent, the energy storage density should be as high as possible, which is determined by the reaction enthalpy of the isomerization and by the molecular weight of the compounds. Consequently, the combination of a high exothermic reaction profile and a low molar mass is desirable. Next to the quantum yield of the photoconversion to the energy-rich valence isomer, the efficiency of this process depends on the overlap of the wavelengths of the incoming light with the absorption spectrum of the energy-lean compound. As the solar spectrum peaks at ~ 550 nm,[8] the absorption maximum should fall in this wavelength range. This often requires the use of suitable photosensitizers and/or the derivatization of the parent molecular framework. Moreover, the long-term stability of the regarded energy-rich molecules, i.e., the half-life time of the photoisomer is crucial for real-life applications in order to avoid spontaneous back reactions. This requirement also implies that the energy-releasing reaction must not be triggered by unintentional stimuli like, e.g., visible light or increased storage temperatures. For both sustainability and economic reasons, a closed energy-storage cycle without significant degradation over time is necessary. In addition, the conditions for upscaling apply as for any other chemical process in industry, that is, the transportation infrastructure should already exist, the turnover numbers can be maximized, and catalyst fouling is prevented. Self-evidently, environmental aspects, availability and costs for synthesis have to be considered. All these, in part conflicting, requirements restrict the utilization of many suggested compound classes. Due to its properties, the molecule pair norbornadiene (NBD) and quadricyclane (QC) appears auspicious concerning its feasibility as MOST energy storage system (see Section 1.2).
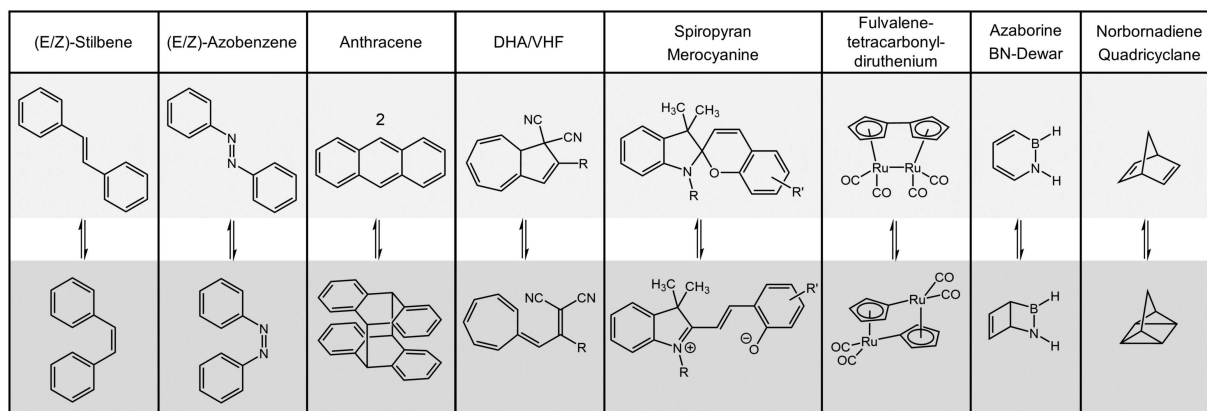
MOST systems can also be considered as molecular photoswitches;[9] in this context, various systems are known in literature (see Scheme 1). The (E/Z)-isomers of stilbene[10] and its derivatives are one of the simplest frameworks, with the energetically higher lying (Z)-configuration being formed by irradiation with light of suitable wavelength. Analogous photoswitches are based on (E/Z)-azobenzene;[11] the photoinduced dimerization of anthracene[12] and the cyclization of linked anthracene dimers[13] also lead to switchable systems. In addition, the isomerization of dihydroazulene (DHA) com-

ChemPhysChem

Review
doi.org/10.1002/cphc.202300806

Chemistry Europe
European Chemical
Societies Publishing

Scheme 1. Listing of different compound classes of molecular solar thermal (MOST) systems with their energy-lean state (light) and the isomerization into their energy-rich state (dark).

pounds to their vinylheptafulvene (VHF)[14] counterparts, and of spiropyran to merocyanine[15] can be utilized. Other examples include organometallic fulvalene-tetracarbonyl-diruthenium[16] complexes, which exist in two different energetic states, as well as azaborine and its BN-dewar[17] isomer. This review specifically focuses on the research regarding the norbornadiene/quadricyclane (NBD/QC)[6e,18] molecule couple due to its particular advantages as potential energy storage material, and addresses the feasibility of various substituted NBD/QC couples.

## 1.2. Photoconversion from Norbornadiene to Quadricyclane

The synthesis of the first norbornadiene (NBD) derivatives was achieved by Diels–Alder reactions,[19] and the production of unsubstituted NBD, through use of cyclopentadiene with acetylene, was patented by Hyman in 1951.[20] Later on, other synthetic routes have been successfully proposed,[21] and insights into the chemistry and reactivity of bridged polycyclic compounds, including norbornadiene and derivatives thereof, became available.[22] While the chemical preparation of a tetracyclic analog was not achieved,[23] the application of photochromism[24] enabled the discovery of the first quadricyclane (QC) derivatives by Cristol *et al.*[25] Shortly afterwards, photoconversion experiments yielded also unsubstituted QC;[26]

Felix Hemauer is a research assistant at Freie Universität Berlin (FU Berlin) and a PhD student at the chair of Physical Chemistry II at Friedrich-Alexander-Universität Erlangen-Nürnberg (FAU), where he received a M.Sc. degree in Molecular Science in 2019. His research is based on synchrotron radiation-based surface science techniques and their use in energy-related topics. His focus lies on the energy release of norbornadiene and quadricyclane derived MOST systems on heterogeneous model catalyst surfaces under well-defined UHV conditions.

Hans-Peter Steinrück is full professor of Physical Chemistry at FAU since 1998. He did his PhD in physics at TU Graz 1985, was postdoc at Stanford University 1985/86, received his habilitation at TU München 1992, and was professor of Physics at Würzburg University from 1993 to 1998. He is member of the European Academy of Sciences, the German Academy of Sciences Leopoldina, the Austrian Academy of Sciences and Academia Europaea, and is Fellow of APS and AAAS. His research focuses on surface and interface science, from ionic liquids, porphyrins, liquid metals, chemical energy storage to chemically modified graphene.
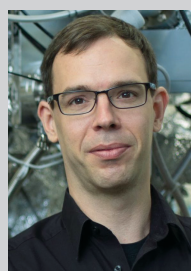
Christian Papp is professor for Applied Physical Chemistry at FU Berlin since 2023. After his PhD at FAU in 2007 and postdoctoral work, he was group leader at FAU. His research aims at the fundamental understanding of surface processes and the analysis of heterogeneous catalysis. Here, the topics range from hydrogen and energy storage to the synthesis and modification of 2D materials. For that surface-sensitive probes, often applying synchrotron radiation, are used.

ChemPhysChem

Review
doi.org/10.1002/cphc.202300806

**Chemistry
Europe**
European Chemical
Societies Publishing

moreover, it was found that utilization of suitable photosensitizers facilitated its formation.[27] Next to photodecomposition reactions,[28] the direct irradiation of NBD with photons became the most accessible route for the synthesis of QC molecules.[23c,29]

Although a complete mechanistic understanding of the isomerization from NBD to QC and its back reaction (see Scheme 2) is not available so far, the interconversion reactions were widely explored by physicochemical methods. The reaction enthalpy, corresponding to the maximum storage energy, is $-89\ kJ\ mol^{-1}$ in the liquid phase,[32] resulting with a molar mass of $92.14\ g\ mol^{-1}$ in a storage density of $0.97\ MJ\ kg^{-1}$, in line with calculated data.[18d] According to the Woodward–Hoffmann selection rules for concerted cycloaddition reactions,[33] the $[\pi 2s + \pi 2s]$ ring opening from QC to NBD[34] is formally forbidden, which explains the rather high activation barrier of $\sim 140\ kJ\ mol^{-1}$.[35] Thus, the stability of the strained metastable QC was found to be surprisingly high, with a half-life of $t_{1/2} > 14\ h$ at 140 °C.[27,36] While the quantum yield of the photoconversion to QC is very low ($\Phi_{isom} = 0.05$),[37] the use of suitable photosensitizers[18b,38] increases this value drastically (highest for acetophenone with $\Phi_{Hg\ lamp} > 0.9$).[39] Hereby, the most efficient route is via triplet sensitization, that is, the triplet energy transfer from the sensitizer to NBD, which then eventually converts to QC.[30,40] The photosensitized isomerization is also promoted by transition metal complexes[41] or semiconductor catalysts.[42]
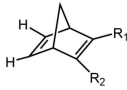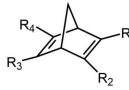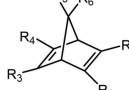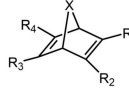
The absorption spectrum of unsubstituted NBD features no major contributions above 300 nm,[29b,43] more specifically, the absorption onset was determined at 267 nm.[44] However, as mentioned above, one prerequisite for the application as

energy storage system is the overlap of the absorption region of the energy-lean molecule with the spectrum of the incoming solar light. Towards this aim, derivatizations of the NBD framework enable the desired bathochromic (redshift) of the absorption onset. Moreover, the utilization of different solvents influences the absorption and conversion characteristics.[45] Another important factor to be considered is the molecular weight of the compounds, in order to ensure a reasonable storage density; the latter should at least outperform the heat stored in solar warming of water (0.2 $MJ\ kg^{-1}$ for $\Delta T = 50\ K$).[18b] As of today, t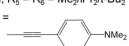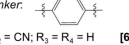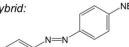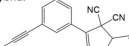uning the properties for optimization of NBD systems led to the syntheses of numerous derivatives; a classification into different classes is shown in Scheme 3. Nevertheless, reliable predictions of the parameters for an applicability as MOST system are difficult, so that further extensive molecular screening is unavoidable.

The approach to optimize the efficiency of the photoconversion of NBD to QC by sunlight is the substitution with electron-withdrawing and -donating groups. These donor-acceptor-derivatives then feature absorption bands in the visible range.[7c] Various substitution patterns are feasible with the NBD skeleton. The derivatization on one side of the framework leads to the extension of the π-conjugation. Tetrasubstituted molecules generate a homoconjugation (through-space interaction) and exhibit high bathochromic shifts; however, the molecular weight is increased significantly reducing the storage densities. Introducing moieties at the methylene bridgehead position has shown to improve quantum yields and the kinetic stability of the QC isomer.[58] The chemistry of hetero-NBDs, especially oxanorbornadiene, is known for several decades;[59] introduction of a heteroatom is
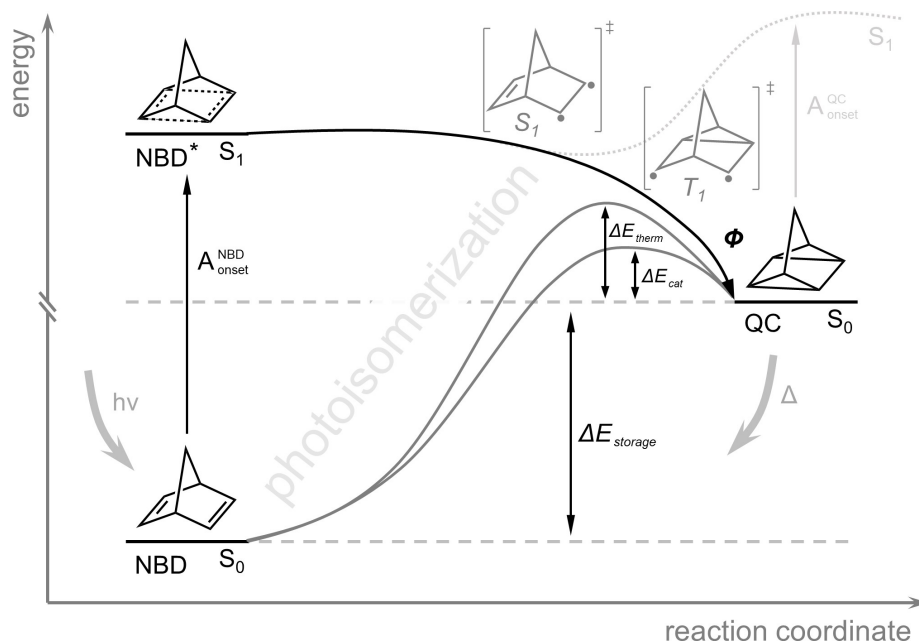
Scheme 2. Depiction of the energy landscape of the photoconversion from NBD to QC. Upon irradiation (hν), NBD is excited to NBD*, which then isomerizes to QC with a particular quantum yield (Φ). The energetic difference between NBD and QC is given by the value of $\Delta E_{storage}$, whereas the activation energy for the back reaction to NBD, under energy release (Δ), is denoted as ΔE_{therm} for thermal and ΔE_{cat} for catalytic routes, respectively. Radical transition states according to Turro et al.[30] Recreated with permission from Ref. [31]. Copyright (2022) John Wiley and Sons.[31]

	Disubstitution	Tetrasubstitution	Bridge Substitution	Hetero NBDs	Linked Systems	Hybrid Systems
Molecule Class	H / R₁ / H / R₂	R₄ / R₁ / R₃ / R₂	R₅ R₆ / R₄ / R₁ / R₃ / R₂	R₄ X R₁ / R₃ / R₂	R₄ Linker / R₃ / R₂	R₄ Hybrid / R₃ / R₂
Substitution & References	$R_1 = R_2 = $ COOMe [7c, 43, 46]; $R_1 = $ COOMe; $R_2 = $ H [46]; $R_1 = $ COOMe; $R_2 = $ Ph [46]; $R_1 = $ Br/Cl; $R_2 = $ Br [47]; $R_1 = R_2 = $ CN [7c, 43]; $R_1 = $ Ph/Ar; $R_2 = $ CN [48, 49]; $R_1 = $ Ph-COOH; $R_2 = $ CN [50]; $R_1 = $ Ph-OMe; $R_2 = $ CN [51]; $R_1 = $ [structure] $R_3 = $ H, OMe, NMe₂; $R_2 = $ CN [44, 45]; $R_1 = R_2 = $ Ph/Ar [6e, 45, 52]; $R_1 = $ Ph; $R_2 = $ CO-CF₃ [53]; $R_1 = $ COOEt; $R_2 = $ Ph [54]	$R_1 = R_2 = $ CN; $R_3 = R_4 = $ Me [7c]; $R_1 = R_2 = $ Ph-OMe; $R_3 = R_4 = $ CN [7c]; $R_1 = R_2 = R_3 = R_4 = $ Ph [55]; $R_1 = R_2 = $ COOEt; $R_3 = R_4 = $ Ph/Ar [56]; $R_1 = $ COOEt; $R_2 = R_3 = R_4 = $ Ph [56]; $R_{3\&4} = $ Ph; $R_1 = R_2 = $ CN [57]; $R_{3\&4} = $ Ph; $R_1 = $ Cl; $R_2 = $ CN [57]; $R_{3\&4} = $ Naphthalene/Anthracene; $R_1 = $ Cl; $R_2 = $ CN [57]	$R_1 = R_2 = $ COOMe; $R_3 = R_4 = $ Ph; $R_5 = R_6 = $ Me [7c]; $R_1 = R_2 = $ CN; $R_3 = R_4 = $ Ph; $R_5 = R_6 = $ Me [37]; $R_1 = R_2 = $ CN; $R_3 = R_4 = $ Ph-OMe; $R_5 = R_6 = $ Me [37]; $R_1 = R_2 = $ COOMe; $R_3 = R_4 = $ Ph; $R_5 = R_6 = $ Me/iPr₂/t-Bu₂ [58]; $R_1 = $ [structure NMe₂]; $R_2 = $ CN; $R_5 = R_6 = $ Me [58]; $R_1 = $ O-CF₃; $R_2 = $ Ph; $R_3 = R_4 = $ H; $R_5 = R_6 = $ Me [53]	$X = $ O; $R_1 = R_2 = $ COOMe; $R_3 = R_4 = $ H [59, 60]; $X = $ O; $R_1 = R_2 = $ CN; $R_3 = R_4 = $ H [59]; $X = $ O; $R_1 = R_2 = $ COOMe; $R_3 = R_4 = $ OMe [61]; $X = $ O; $R_1 = R_1 = $ Bn-OMe; $R_3 = R_4 = $ H [62]; $X = $ N-H/N-COOMe; $R_3 = R_4 = $ H [63]; $X = $ N-CH₃/N-Bn; $R_1 = R_2 = $ COOH; $R_3 = R_4 = $ H [59]; $X = $ Si-(CH₃)₂/Si-(Ph)₂; $R_1 = R_2 = R_3 = R_4 = $ H [59]	*Linker:* But-2-yne; $R_2 = $ CN; $R_3 = R_4 = $ H [64]; *Linker:* [structure]; $R_2 = $ CN; $R_3 = R_4 = $ H [6e, 64]; $R_2 = $ CO-CF₃; $R_3 = R_4 = $ H [65]; *Linker:* Thiophene; $R_2 = $ CN; $R_3 = R_4 = $ H [66]; *Linker:* [carbazole structure]; $R_2 = $ CN; $R_3 = R_4 = $ H [66]	*Hybrid:* [structure] —NBD'; $R_2 = $ CHO/CH=C(CN)COOC₂H₅; $R_3 = R_4 = $ H [67]; *Hybrid:* [structure] NC CN; $R_2 = $ Ph/CN; $R_3 = R_4 = $ H [68]
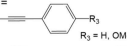
Scheme 3. Overview of various exemplary derivatives of NBD (selection), categorized into different molecule classes depending on their functionalization. The syntheses and resulting properties are described in the corresponding literature.

expected to enhance the storage properties of the respective molecule pair.[69] Another strategy is to link NBD units creating systems with an array of photoswitches.[64,66] Similarly, multiple MOST molecules can be fused generating hybrid systems with advantages of both compound classes.[67–68]

Based on these substitution patterns, an enormous catalog of derivatives of the NBD framework is synthetically available using different substituents. Early derivatization was carried out with ester moieties, dating back to the discovery of first NBD molecules.[19,46] Later on, utilizing donor-acceptor systems with cyano and methyl groups, the absorption onset was shifted by above 100 nm to higher wavelengths, while maintaining a reasonable molecular weight.[7c] More elaborated systems, e.g., various diarylnorbornadienes,[56] feature even better absorption properties, improved stabilities, and preferential reaction kinetics. In addition, attaching methyl groups or bulkier moieties at the bridgehead leads to new derivatives with improved characteristics.[37,53, 58]
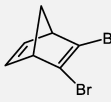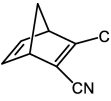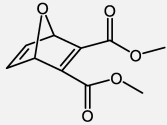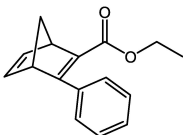
By tendency, there is a trade-off between redshift of the absorption onset of an NBD derivative and the molecular weight of the compound. Moreover, the quantum yields and extinction coefficients are also affected by the derivatization and have to be taken into account. For instance, the *bis(pentaamineruthenium(II))* complex of dicyano-norbornadiene shows a distinct shift of the absorption onset towards $\sim$ 700 nm; however, small photoconversion yields ($\Phi_{500\ nm} = 8.3 \times 10^{-4}$) and the high molecular weight ($M = 515.5\ g\ mol^{-1}$ only for the cationic complex) make the system not applicable for energy storage.[70] Altogether, considering the size and electronic properties, the 2,3-disubstitution of NBD appears to be most viable for solar storage applications. Alongside symmetric substitution patterns,[7c,43, 46] there are diverse reported syntheses for differently functionalized molecules with push-pull substituents, especially promoted by the group of Moth-Poulsen et al. in the last few years.[44–45,48–49, 51–53]

The photoconversion, i.e., energy storage, from the NBD to the QC derivative is the first step and a prerequisite for an applicable system. The conversion parameters (absorption onset, extinction coefficients, quantum yields, selectivity) are benchmarked to get an idea of the overall efficiency and have to be put into context with the obtained kinetic stabilities and energy storage densities of the QC derivatives for a potential application. For the later presented surface science studies (see Table 1), the quantitative reaction to the energy-rich photo-isomer was ensured by NMR measurements, or the light-induced isomerization was followed *in situ* by appropriate experiments. For all experimental conditions, i.e., liquid phase or UHV, no changes in the conversion mechanism were observed. The unsubstituted molecule pair, NBD and QC, was explored in detail on a Pt(111) surface (see Section 2.1), whereby high conversion was achieved with a suitable sensitizer. Derivatization oftentimes enables a direct photoconversion without sensitizers, reducing unwanted side or follow-up reactions. Moreover, the enhanced absorption properties with regard to the solar spectrum encourages the use of NBD derivatives.
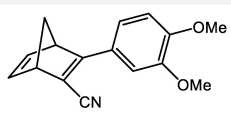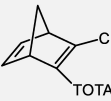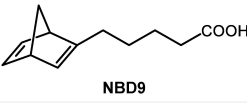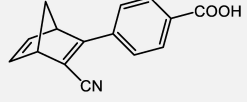
In the plethora of synthetically available derivatives, an assessment of promising molecules with optimized properties for energy storage applications is necessary, particularly due to the expected complexity of the interconversion of substituted NBD/QC molecules.[18d] For this purpose, quantum mechanical modelling gives important predictions of desired trends. First-principle calculations were performed by Kuisma et al. regarding the optical and thermal behavior of various donator and acceptor substituents in NBD/QC systems.[71] In general, there was a compromise between the spectral match with the solar spectrum and the storage density, as there was a relation between the induced bathochromic shifts of the absorption onset and the mass of the substituent. Moreover, for large redshifts (more pronounced for electron-accepting moieties), next to decreased thermal stabilities, the corresponding QC isomer also featured absorption bands in the visible light range, inducing unwanted back conversions and reactions. Thus, single-substituted derivatives appeared interesting for further investigation. Besides, the importance of solvent and vibrational effects was stressed. Other theoretical calculations included the effects of externally applied forces on the NBD/QC framework to model steric contributions of substituents.[72] Thereby, an

Table 1. Considered NBD derivatives, with their respective absorption onsets (λ_{Onset}), and the utilized substrate for energy release; the adsorption geometry is given, when known. Next to the stability limits, the feasibility and conditions of the energy release of the corresponding QC isomers are listed. Derivatized NBD molecules are always written in bold.

MOLECULES	λ_{Onset}	SURFACE	ENERGY RELEASE	ADSORPTION	STABILITY	REF.
NBD	267 nm	Pt(111) + sensitizer (MK) Ni(111)	at 125 K or 0.32 V_{fc} at ~168 K	η^2:η^1 n/a η^2:η^2	thermal: 190 K 96% selectivity thermal: 190 K	[94] [95] [97]
NBD2	n/a	Ni(111)	at 170 K	"side-on" Br away	partial dissoc. (at 120 K), thermal: 190 K	[106]
NBD3	345 nm	Ni(111)	at 175 – 260 K	η^2:η^2	thermal: 290 K	[107]
NBD4	332 nm	Pt(111)	at 310 – 340 K $k = 5.3\times10^{-4}\ s^{-1}$	"side-on"-like (bridge oxygen towards surface)	thermal: 380 K > 99% selective	[109]
NBD5	359 nm	Pt(111) Ni(111) Au(111) HOPG	at 140 – 230 K / instantaneous for ≥ 0.5 V_{fc}	no "side-on" oxygen-bound upright standing n/a	thermal: 300 K thermal: 160 K desorption: 250 K 60% selectivity	[112] [112] [113] [114]
NBD6	380 nm	HOPG	for ≥ 0.3 V_{fc} completed at 0.4 V_{fc}	n/a	≥ 99.3% selectivity (electrochemical)	[114]
NBD7	389 nm	Pt(111) HOPG Au(111)	0.02 – 0.92 V_{fc} 0.02 – 0.82 V_{fc} $k = 2\times10^{-4}\ m\cdot s^{-1}$	n/a n/a n/a	> 99% reversible 99.8% reversible > 1000 cycles	[115] [116] [117]
NBD8	310 nm	Au(111)	instantaneous (monolayer)	TOTA in plane, NBD anchored	desorption: 320 K (multi) 600 K (mono)	[121]
NBD9	n/a	Co$_3$O$_4$(111)	n/a	anchored (chelating), flat/standing	desorption: 240 K (multi) thermal: 400 K	[122]
NBD10	378 nm	Co$_3$O$_4$(111)	thermal barrier: 103 kJ mol^{-1} (350 – 370 K)	anchored (chelating)	desorption: 280 K (multi) thermal: 570 K 98.5% reversible	[50] [123]
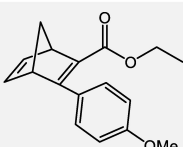
increase in the stored energy (up to 70 $kJ\ mol^{-1}$) and the modification of the activation energy was achieved. Recently, the screening of 3230 NBD/QC derivatives was conducted with the use of extended tight binding (xTB) methods. A sufficient correlation between results from DFT and the obtained information on reaction and storage energies as well as reactant and product absorption was demonstrated.[73] To screen an even higher number of kinetically stable NBD derivatives with suitable properties, machine learning methodologies were applied.[74]

1.3. Cycloreversion from Quadricyclane to Norbornadiene

Next to the search for tailoring a suitable molecule pair itself, the energy release from the QC derivative has to occur in a controlled and efficient way. Hereby, the back conversion to its corresponding NBD isomer can be achieved in a thermal, catalytic, or electrochemical manner. As mentioned above, the symmetry rules for a concerted ring-opening reaction[33a] lead to the observed energetic barrier for the backward isomerization of QC to NBD, visualized in the energy landscape of the conversion (see Scheme 2). This thermal pathway has early been explored successfully (above 150 °C in the gas phase),[35] with the determination of the respective heat of isomerization.[32b] However, the release of the stored energy is usually needed during times of energy-deficiency. Utilizing heat to trigger the cycloreversion to NBD gives low overall efficiencies and thus is not the preferred route for back conversion. Besides, gas-phase experiments on a QC carboxylate derivative stated a collision-induced back reaction to its relaxed isomer to be possible.[75]

Transition metals, e.g., rhodium, platinum[36] or nickel,[76] are known to catalyze the rearrangement of cyclic organic molecules,[77] with the choice of the ligands playing an important role.[78] Different mechanisms for the catalytic energy release are discussed in literature:[79] the concerted mechanism involves the change of symmetry constraints by complexation,[80] for the Lewis acid type the transition via a metallocarbonium ion is found,[81] and the oxidative-addition reaction path includes the formation of a metallocyclic intermediate.[82] Among others, the reduction of Ag(I) salts was found to promote the rearrangement of QC to NBD in solution.[83] Needless to say, different electronic and steric characteristics of the particular QC derivatives require for accordingly adapted catalyst materials.

An alternative route for the energy release from QC follows an electrochemical approach. The oxidation of QC occurs readily (0.91 V vs. SCE)[84] and facilitates the back conversion to NBD, whereby the energetic barrier is lowered by more than 100 kJ mol^{-1} for the isomerization between the radical cation species.[85] While the isomerization can be triggered via a redox-mediated chain mechanism,[86] observed electrode fouling and unwanted side reactions reduce the chemical efficiencies.[87] Therefore, photoelectrochemical approaches tackle the issue of limited control in the process.[88] Ultimately, the aim is to gain the stored energy of a MOST system not as heat but in form of electricity. For that, a coupling to a semiconductor material as electrode is necessary (see Scheme 4).

With the advantage of a straightforward separation of the reaction product, simple recycling, and a huge variety of materials, heterogeneous catalyst concepts are preferable for large-scale applications. Moreover, liquid MOST systems demand for heterogeneous catalysis to enable an energy release that proceeds fast enough.[31] The implementation into suitable storage devices then involves the tailoring of the combination of molecule system and appropriate catalyst for an optimized performance. Mechanistic insights into the surface processes during the reactions are needed in order to understand and
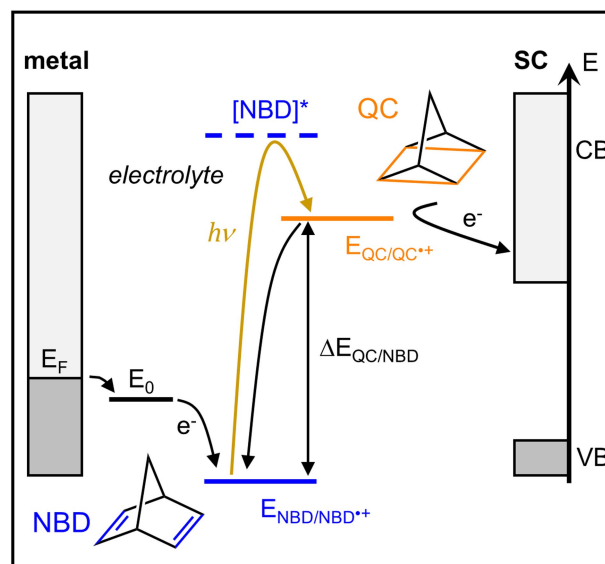
Scheme 4. Energy release from QC in form of electricity in a photo-electrochemical mechanism, proposed by Brummel et al.[88] Photoconversion of NBD to QC (over transition state [NBD]*), electron transfer to conduction band (CB) of a semiconductor material, and charge compensation by a metal. The difference of the thermodynamic electron energies is denoted as $\Delta E_{QC/NBD}$. Recreated with permission from Ref. [88]. Copyright (2016) John Wiley and Sons.[88]

improve the catalytic activity.[89] Surface science experiments under well-controlled ultra-high vacuum (UHV) conditions allow for fundamental model studies of potential molecule pairs; in this way, the objective is the knowledge transfer to real-life applications under operation conditions. Information on the energy-releasing cycloreversion reaction from the respective QC to NBD derivative is particularly crucial in the search for promising molecule and catalyst design. Besides, adsorption geometries and interaction strengths with the surface, thermal stability boundaries and decomposition pathways, and desorption processes are of interest to promote the selection of suitable MOST systems.

In the following, this review gives an overview of surface science investigations on NBD/QC systems. Please note that findings of different spectroscopic techniques, mainly XPS and IRRAS measurements, corroborated by DFT calculations, are included; as comparable UHV conditions and well-defined model surfaces were utilized, the main results can be contextualized and their trends identified. We begin with the exploration of the unsubstituted NBD/QC molecule pair. Here, studies on the surface chemistry on various catalyst surfaces and insights into the electrochemical behavior are presented. Thereafter, research findings on differently 2,3-substituted NBD derivatives and their corresponding QC isomers are addressed, with a classification into symmetric and asymmetric compounds. Where respective data are available, both the catalytically and electrochemically triggered energy releases are described. Finally, the applicability of NBD derivatives is demonstrated in MOST-based devices, whereby the current state of the art is pointed out by implementations of exemplary

molecules, which are structurally related to the introduced compounds.

2. Surface Science of Norbornadiene and Quadricyclane Derivatives

2.1. Unsubstituted NBD/QC

The parent NBD/QC pair is, due to its small molecular size, the simplest model system for surface science studies. First, Muetterties et al. discovered a high sticking coefficient for NBD on Pt(111) at room temperature and the evolution of benzene and hydrogen at elevated temperatures above 520 K.[90] From isotopic labelling the incorporation of the bridgehead CH_2 into the desorbing benzene was excluded, indicating a regioselective removal of the bridging carbon.[91] Further investigations on the adsorption and reaction behavior of NBD on Pt(111) were conducted by Hostetler et al. with infrared reflection absorption spectroscopy and complementary methods.[92] An $\eta^2:\eta^1$ binding motif was found at low temperatures of 130 K, i.e., the coordination of only one C=C double bond with the surface and an agostic interaction of the bridgehead CH_2 subunit with the substrate. This agostic C–H bond was cleaved upon heating to 260 K, resulting in a norbornadienyl species, which was stable up to 450 K. The decomposition was suggested to proceed via a retro-cyclization yielding benzene and hydrocarbon residues, as reported before.[90–91] Photoionization mass spectrometry measurements in the 7-22 eV energy range determined the ionization potentials and energies for ionic fragmentation; before the formation of $C_7H_7^+$, the interconversion of NBD and QC ions was concluded.[93]

An electrochemical characterization of both molecules yielded the oxidation potentials, with a difference of 0.61 V (corresponding to 59 *kJ mol^{-1}*) as maximum theoretical electrical output. Follow-up infrared spectroscopy studies, supported by DFT calculations, analyzed the vibrational properties of the NBD/QC pair, and allowed for the unambiguous spectroscopic assignment of the two valence isomers. Electrochemical IR experiments, using Pt(111) as working electrode, traced the oxidation reactions and the formation of NBD, and demonstrated the potential control of the reaction rate of the exothermic cycloreversion.[88]

The surface chemistry of NBD and QC on a Pt(111) substrate was addressed in detail by Bauer et al. in a combined XPS, UPS, IRRAS, and DFT study.[94] The chemisorption of NBD at low temperatures of 125 K was investigated by IRRAS data and, after comparison with calculated spectra, confirmed to proceed in an $\eta^2:\eta^1$ geometry (see Figure 1). For the first time, also the reaction behavior of QC on a surface was directly assessed. In the multi-method approach, the rapid cycloreversion reaction of QC to NBD already at 125 K was deduced from an identical spectral appearance. Notably, in the multilayer, which is not in direct contact to the platinum model catalyst, the energy-rich QC was found to be stable, as concluded from clearly distinguishable spectroscopic characteristics of QC and NBD. After multilayer desorption upon heating until 160 K, the detection of only NBD in the remaining monolayer was in line with the instantaneous conversion of QC to its energy-lean isomer on Pt(111). In addition, the catalytic activity was demonstrated by exposure of a precovered surface to QC; the isomerization of the QC species only occurred at direct contact with the platinum. The findings on the thermal evolution of NBD supported the cleavage of the agostic C-H bond between 190 and 200 K, resulting in a directly bound carbon atom of the methylene bridgehead; this norbornadienyl species was stable up to 380 K. At higher temperatures, further dehydrogenation and fragmentation of the carbonaceous framework was suggested, while, in contrast to previous literature, no benzene and methylidyne (CH) was formed.
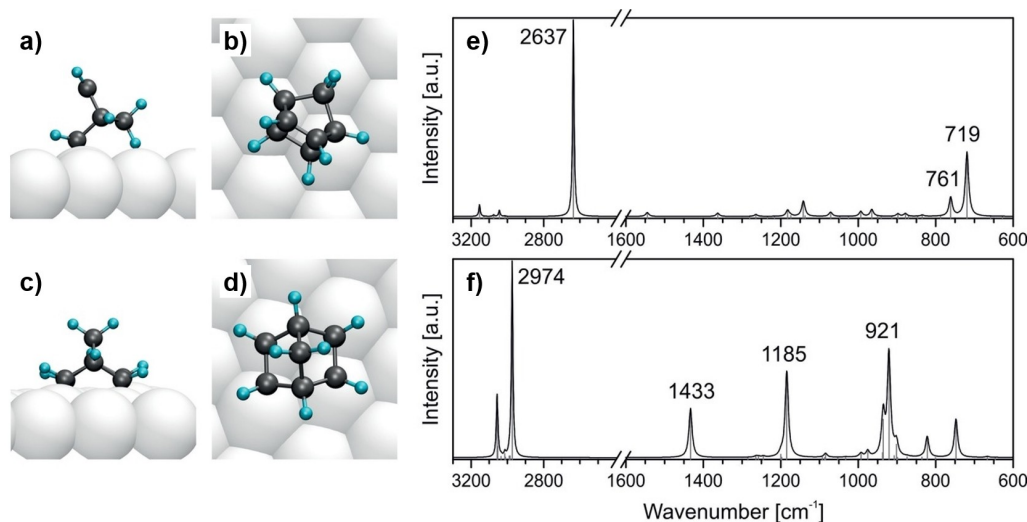

Figure 1. Possible adsorption geometries of NBD on Pt(111): (a) $\eta^2:\eta^1$ (side view), (b) $\eta^2:\eta^1$ (top view), (c) $\eta^2:\eta^2$ (side view), and (d) $\eta^2:\eta^2$ (top view); corresponding calculated IR spectra are depicted in (e) for $\eta^2:\eta^1$ and (f) for $\eta^2:\eta^2$ motifs. Adapted with permission from Ref. [94]. Copyright (2016) John Wiley and Sons.[94]

ChemPhysChem

Review
doi.org/10.1002/cphc.202300806

Chemistry Europe
European Chemical
Societies Publishing

In a subsequent study, photoelectrochemical IRRAS (PEC-IRRAS) investigations were carried out by Brummel *et al.*, combining the photochemical conversion of NBD to QC and the electrochemically triggered cycloreversion of QC in one experiment.[95] In this way, the overall reversibility of the energy storage cycle became available. Again, Pt(111) was used as working electrode in a three-electrode setup, whereby the measurements were performed in acetonitrile (MeCN) in a thin-layer configuration (with an electrolyte film thickness of approximately 4 μm). For the isomerization of NBD to QC, Michler's ketone (*4,4'-bis(dimethylamino)benzophenone, MK*) was chosen as photosensitizer, which exhibits an absorption maximum close to the employed high-power UV LED (365 nm). After having determined the extinction coefficients of characteristic vibrational bands, the concentrations during conversion from NBD to QC upon irradiation were calculated (see Figure 2a), giving a final conversion of 80% with an effective external quantum yield of 1.5% at 365 nm and short photoconversion times (560 ms); thereby, the initial selectivity was found to be 95%, which decreased over time (see Figure 2b) and was probably limited by unwanted follow-up reactions between the photosensitizer and QC. The electrochemically triggered backward reaction to NBD was monitored as function of the applied potential. Due to the above-mentioned catalytic activity of platinum, part of QC was directly converted to NBD (< 20%). Between 0.02 and 0.52 V_{fc}, the remaining QC was consumed completely at the expense of formed NBD. While the onset of the oxidation of NBD was detected above 1.0 V_{fc}, the characteristic potential for QC was confirmed to be 0.32 V_{fc} (see Figure 2d). The decomposition of the photosensitizer, at around 0.42 V_{fc}, marked one of the most limiting factors. Otherwise, the

high selectivity of the cycloreversion reaction to NBD (96%) indicated no major side reactions.

Schwarz *et al.* performed *in situ* photochemical studies on the NBD/QC system by IRRAS under UHV conditions.[96] Different mixtures of the photosensitizer MK and NBD were coadsorbed on Pt(111) at 120 K. Using a ratio of NBD/MK (7.4 : 1), quantum yields of up to 23% at 365 nm were reached for the photoconversion to QC, while an initial selectivity of 70% was observed. Among others, substrate-induced effects and phase separation caused a decrease of the efficiencies, in particular for either very small or high NBD coverages. The experiments on photoreactions with low quantum yields and in thin-film configuration were possible through an UHV-compatible high-intensity UV-photon source with high photon flux densities (2×10^{18} s^{-1} cm^{-2}) at a wavelength of 365 nm.

Having explored the fundamental surface reactions on Pt(111), analogous investigations were carried out on the less reactive Ni(111) surface as catalyst substrate to gain control over the energy release.[97] Again, a multi-method approach led to information on the feasibility of the energy release of the system, and to the proposal of a reaction pathway of the molecule pair NBD/QC. Synchrotron radiation-based XPS and UPS measurements demonstrated the intact adsorption of both molecules on Ni(111) at ~120 K and a clear spectroscopic distinction of the isomers. DFT calculations for NBD showed that, in contrast to the above-discussed side-on (η^2:η^1) adsorption geometry on Pt(111), a flat binding motif (η^2:η^2) is energetically favored on Ni(111). Corresponding NEXAFS measurements of NBD confirmed the parallel alignment of the double bonds. Notably, the calculations for QC exhibited similar energies for both geometries. The higher reaction energy (215 $kJ\,mol^{-1}$)
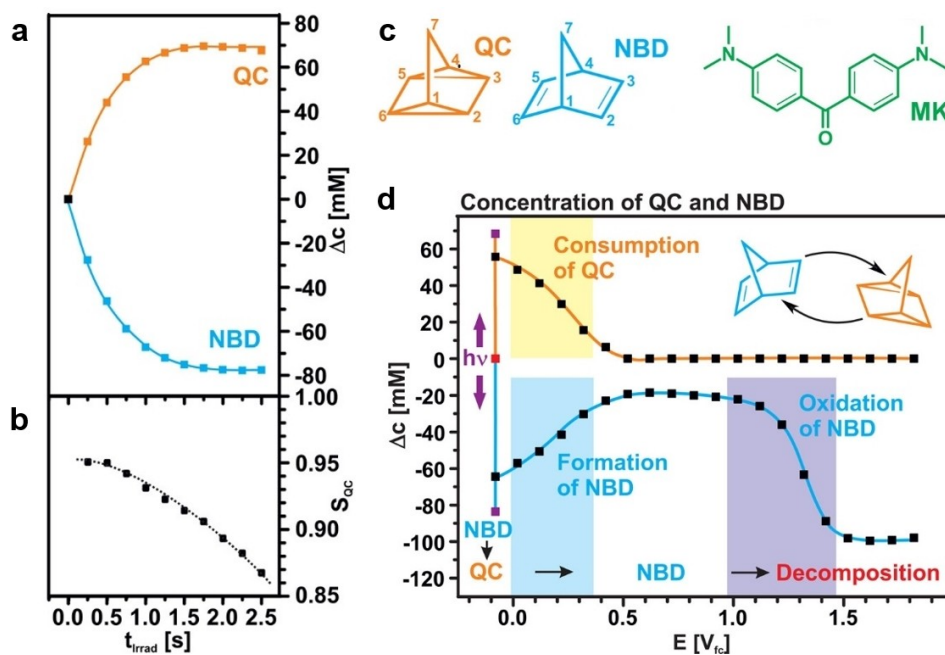
Figure 2. (a) Photoinduced isomerization of NBD to QC (0.1 M NBD with 20 mM MK in acetonitrile) as function of irradiation time. (b) Decline of selectivity of photoconversion over time. (c) Molecular structures of QC, NBD, and Michler's ketone (MK). (d) Changes of concentrations during photochemical isomerization to QC and electrochemically triggered cycloreversion back to NBD in dependence of the applied voltage. Adapted with permission from Ref. [95]. Copyright (2017) American Chemical society.[95]

from QC to NBD on Ni(111), compared to the gas phase (89 *kJ mol^{-1}*), was determined due to the stronger interaction of NBD with the surface than QC; however, in the scope of a catalytic cycle, the subsequent desorption is also hindered thereby. Temperature-programmed experiments showed the identical spectral appearance for both molecules at 175 K. In comparison to the rapid reaction of QC to NBD on Pt(111),[94] the catalytic energy release occurred in a controlled manner at higher temperatures. The thermal stability of NBD was given up to 190 K, as for Pt(111), after which the decomposition into benzene and methylidyne (CH) was monitored. Above 330 K, the fragmentation into unspecified C—H fragments and, finally, carbide was proposed (see Figure 3). To avoid the detrimental degradation of the NBD molecules on the catalyst surfaces, different substituents have been evaluated (see below) that influence the adsorption and reaction behavior. Besides improved storage properties and efficiency reasoning, the objective is to achieve higher thermal stability limits of the respective NBD derivatives.

Next to the discussed publications, various spectroscopic characterizations of NBD and QC have been conducted in the last years. Rotationally-resolved infrared absorption spectra of NBD were measured and assigned, including the determination of the respective spectroscopic constants based on fitting.[98] In a series of studies, Palmer *et al.* performed synchrotron-based experiments in the gas phase and corresponding elaborated calculations in order to gain insights into the ionic states of NBD and QC,[99] the singlet and triplet valence states of NBD,[100] and also the singlet states of QC,[101] which are of interest during the interconversion of both molecules. In addition, latest theoretical approaches unveiled the importance of considering Rydberg excited states and dynamic electronic correlation effects in calculations for photorelaxation pathways within the

NBD/QC system.[102] Moreover, the excited-state deactivation mechanism of NBD was investigated in a full computational study.[103] Recently, a newly integrated multipole ion trap at PETRA III was tested with NBD by ion-impact ionization. Alongside the fragmentation to, most of all, NBD ions ($C_7H_x^+$), the reaction of NBD with the generated ions led to the detection of heavier products up to $C_{12}H_x^+$, with the largest peak for $C_9H_x^+$ after the transfer of acetylene from a neutral NBD molecule.[104]

In summary, the surface chemistry of unsubstituted NBD dates back to model studies on Pt(111), giving insights into its adsorption motif and thermally induced reaction pathways. Experiments on the corresponding photoisomer QC revealed a high catalytic activity of platinum, so that the energy-releasing back reaction to NBD was triggered upon adsorption at low temperatures or by applying an oxidative potential. Utilizing Ni(111) as catalyst material, the cycloreversion from QC to NBD was achieved at higher temperatures, whereby the thermal stability limits were comparable to Pt(111). Although the underivatized system exhibits the highest energy storage density, the photoconversion from NBD to QC is not facile without sensitizer.

2.2. Substituted NBD/QC Systems

As discussed in the introduction, a suitable derivatization of the parent NBD framework enables higher efficiencies as MOST system, in particular through a better overlap with the incoming solar spectrum by a redshift of the absorption maximum of the NBD molecule. Moreover, due to electronic and steric reasons, and different adsorption motifs, a deviating reaction behavior of the substituted molecules is anticipated on the considered surfaces, ideally, resulting in an enhanced stability on the
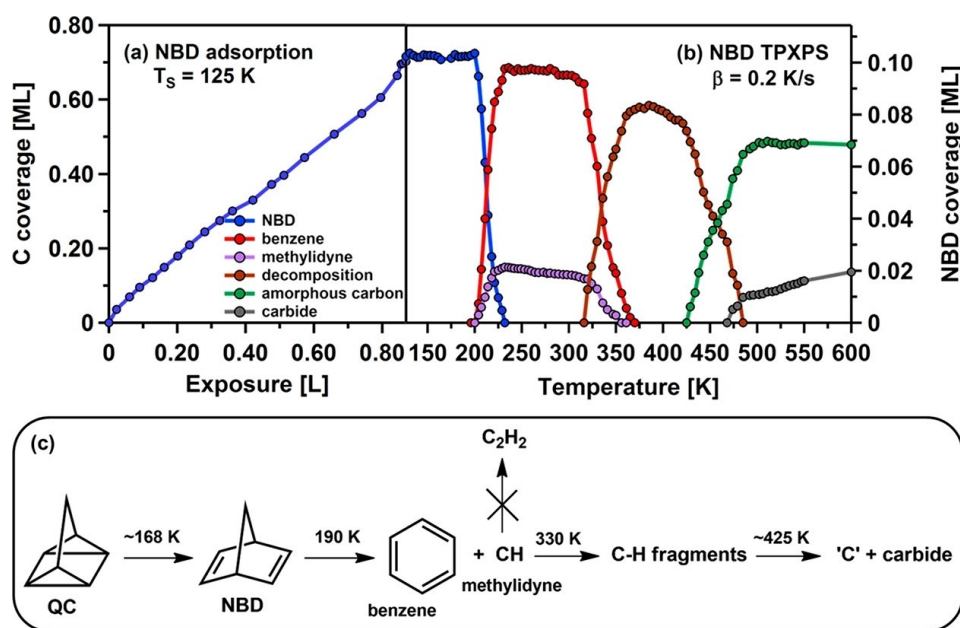

Figure 3. Quantitative representation of respective surface species as function of (a) exposure during adsorption of NBD on Ni(111) and (b) temperature in the course of the temperature-programmed XPS (TPXPS) experiment. (c) Proposed reaction pathway of QC adsorbed on Ni(111). Reprinted with permission from Ref. [97]. Copyright (2019) American Chemical Society.[97]

catalyst. An overview of conducted surface studies on various derivatives is given in Table 1.

2.2.1. Symmetric 2,3-Substitution of NBD/QC

The symmetric substitution with electron donating moieties is expected to yield higher storage capacities by an increased energetic difference of both isomers.[105] Analogous to the unsubstituted NBD/QC system, Bauer *et al.* investigated the surface chemistry of 2,3-dibromo-NBD (**NBD2**) as first simple model system on Ni(111) with HR-XPS and UPS.[106] In addition, findings on the adsorption geometries were gained by DFT calculations (see Figure 4). Due to the bulky bromine moieties, a strong interaction of the sp^2 carbon atoms of NBD with the surface is hindered. Therefore, the most stable configuration was found to be a side-on binding motif with the Br atoms being oriented away from the surface (Figure 4a). Yet, the cleavage of the Br bonds upon adsorption was favorable, as the dissociation of bromine would lead to increased adsorption energies. In contrast, **QC2** exhibited the most stable adsorption geometry with the Br atoms pointing towards the surface (Figure 4c and 4d). A detachment of the bromine is less likely, since the bond is more stable at a sp^3-hybridized atom, and the distance between the carbon atoms and the surface is larger.

Adsorption experiments on Ni(111) at temperatures about 120 K showed that both **NBD2** and **QC2** were clearly distinguishable by XPS measurements in the C 1s region with their unique spectroscopic fingerprint; in the Br 3d region, two separated doublets were observed for the two isomers, respectively, revealing different bromine species, including the partial dissociation of the molecules upon adsorption. In accordance with the calculations, the amount of atomic Br was lower for **QC2**, indicative of a higher stability of the C–Br bond. The thermal evolution demonstrated the conversion of **QC2** to **NBD2** at 170 K. However, since the molecules are only partially

stable on the surface, it was assumed that also the reaction route towards parent NBD took place to a significant extent. Thus, the dissociation of Br from **QC2** occurred alongside with the onset of the cycloreversion reaction at 130 K. For **NBD2**, when heating to above 190 K, benzene and methylidyne were detected as decomposition products, similar to the observations for unsubstituted NBD; simultaneously, the cleavage of remaining bromine moieties was monitored (see Figure 5). The spectral distinction was also possible in complementary UPS experiments. Above 200 K, the identical reaction pathways led to equivalent spectra. Moreover, the authors found prolonged irradiation with X-rays as alternative trigger for the cycloreversion step.

As follow-up study, the reaction behavior of 2,3-dicyano-NBD (**NBD3**) and its energy-rich counterpart was explored on Ni(111), since with cyano substituents a higher stability of the molecules was expected.[107] The cyano group is known to act as pseudohalogen but has a lower molecular weight and higher bond strength. Consequently, intact adsorption along with controlled energy release was anticipated. Indeed, at low temperatures of 130 K, HR-XPS spectra indicated the molecular adsorption of both isomers without any signs of dissociation. DFT calculations provided again the most probable geometries: **NBD3** was found to bind most strongly in a flat (η^2:η^2) configuration, while **QC3** had similar adsorption energies for both flat and side-on (η^2:η^1) motifs. Simulated XP spectra were in line with the experimental data concerning the characteristic spectroscopic fingerprints in the C 1 s and N 1 s regions of the molecule pair. Upon heating, subtle changes in the relative peak intensities were ascribed to a rearrangement step of **NBD3** on the surface; it was suggested that thereby the energy barrier for this transition into its most stable geometry has to be overcome. For **QC3**, the cycloreversion was triggered starting at 175 K, with complete conversion to **NBD3** until 260 K, without any side reactions. The molecular framework was stable up to 290 K, exceeding the stability range of unsubstituted NBD
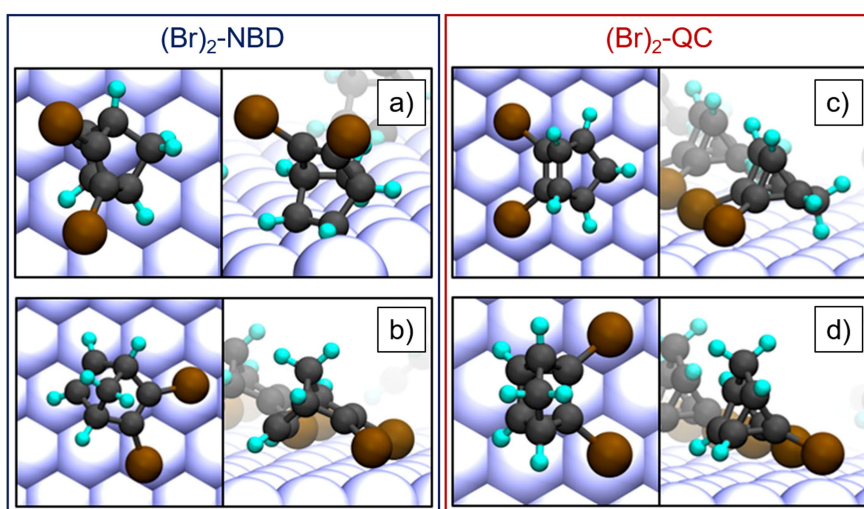
Figure 4. Depiction of adsorption motifs (top and side view), calculated for (Br)$_2$-NBD (**NBD2**) and (Br)$_2$-QC (**QC2**) on Ni(111) with the highest stability: (a) **NBD2** side-on Br away, (c) **QC2** side-on Br on-top, and (d) **QC2** flat Br on-top; (b) **NBD2** flat Br on-top shown for comparison; on-top positions of Br were determined to be more stable than bridge sites. Adapted with permission from Ref. [106]. Copyright (2019) AIP Publishing.[106]

ChemPhysChem

Review
doi.org/10.1002/cphc.202300806

Chemistry
Europe
European Chemical
Societies Publishing

Figure 5. Quantitative representation of respective surface species in both core levels (C 1 s and Br 3d) as function of (a, c) exposure during adsorption of Br$_2$-QC (**QC2**) on Ni(111) and (b, d) temperature in the course of the temperature-programmed XPS (TPXPS) experiment. Adapted with permission from Ref. [106]. Copyright (2019) AIP Publishing.[106]

system by far. Contrary to earlier studies on Ni(111), no benzene or methylidyne was detected; instead, the detachment of the cyano moieties and the fragmentation into unspecified carbonaceous fragments was proposed. Above 400 K, only amorphous carbon, carbide, and nitride remained on the surface (see Figure 6). Overall, the controlled quantitative isomerization at comparably high temperatures was assessed as advantageous.

The same NBD derivative, 2,3-dicyano-NBD (**NBD3**), has also been surveyed regarding its pure rotational spectrum in the 75–110 GHz range, yielding the respective spectroscopic constants.[108]

The previously discussed NBD/QC systems exhibited a pronounced involvement of the methylene bridgehead group: While on Pt(111), the 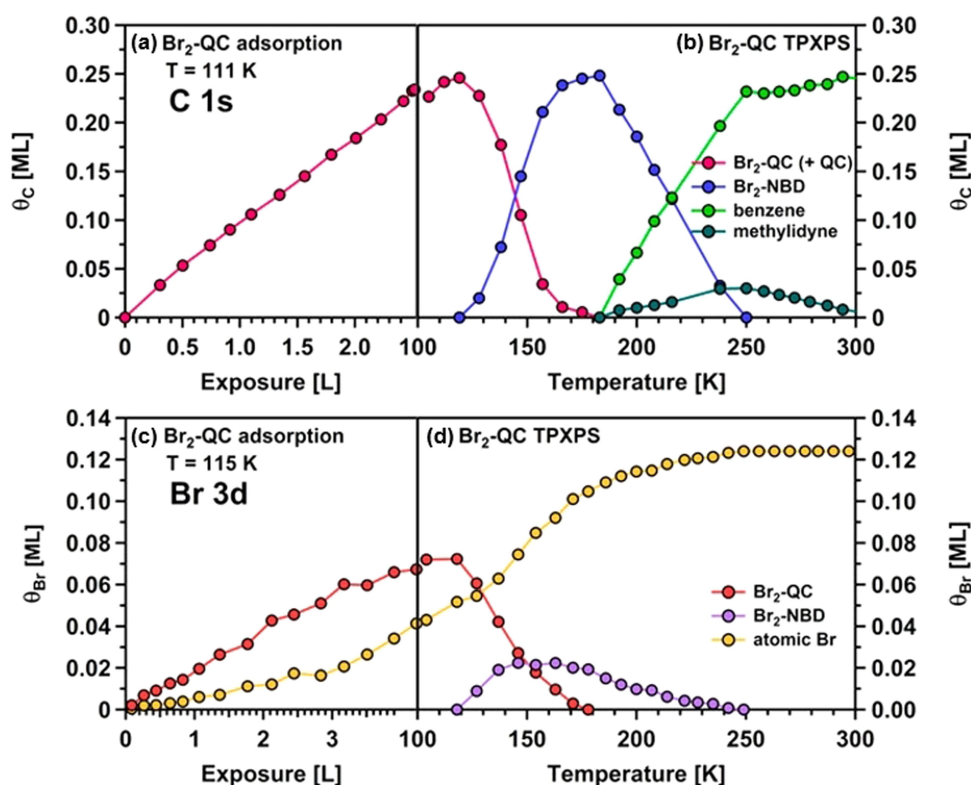unsubstituted NBD undergoes an early decomposition step through the agostic C–H interaction between the CH$_2$ bridgehead and the surface,[94] on Ni(111) the formation of benzene implies the detachment of the bridging carbon atom.[97,106] Thus, this position marks another possibility for molecular adjustments. Moreover, as outlined in the introduction, moieties at the bridgehead give advantageous properties for MOST system applications. The introduction of an oxygen atom at the bridgehead position was expected to lead to different adsorption geometries and surface reactions. As
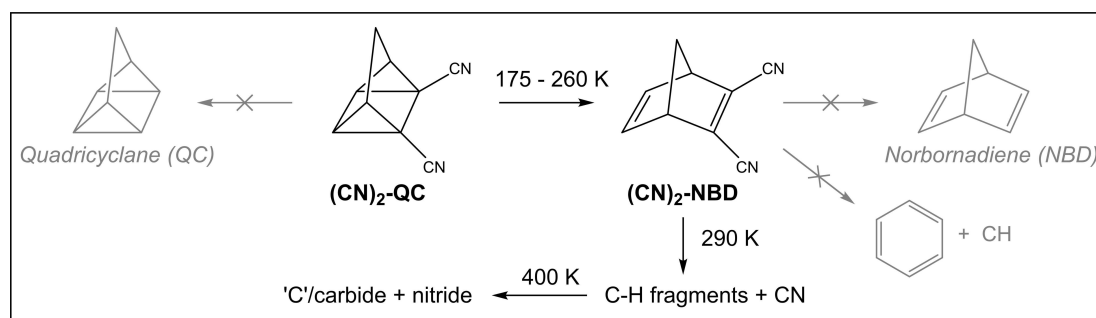
Figure 6. Surface chemistry of (CN)$_2$-QC (**QC3**) on Ni(111), as deduced from *in situ* TPXPS: quantitative cycloreversion into (CN)$_2$-NBD (**NBD3**), subsequent decomposition into C–H fragments and CN, and final formation of amorphous carbon, carbide, and nitride. Reprinted with permission from Ref. [107]. Copyright (2022) John Wiley and Sons.[107]

ChemPhysChem

Review

doi.org/10.1002/cphc.202300806

Chemistry
Europe

European Chemical
Societies Publishing

first surface study on a hetero-NBD/QC, different ester derivatives of oxa-NBD/QC were investigated on Pt(111).[109] Notably, for these systems one expects the superposition of the influences induced by the oxa-NBD subunit and the attached ester substituents of different lengths. Temperature-programmed XPS (TPXPS) measurements proved the successful cycloreversion of 2,3-bis(methylester)-oxa-QC (**QC4**) to its corresponding energy-released isomer **NBD4** above 310 K. At lower temperatures, rearrangement steps were proposed for both molecules upon heating. The thermal stability limit of **NBD4** was found at ~380 K, after which the formation of C−H fragments and carbide was observed. The comparison with larger-extended 2,3-bis(benzylester) derivatives showed an early decomposition of those molecules already at only 135 K, yielding, among fragmented species, carbon monoxide (CO) on the surface. Complementary photochemical infrared reflection absorption spectroscopy (PC-IRRAS) experiments in the liquid phase confirmed the catalytic activity of Pt(111) for the conversion of the oxa-QC derivatives under more realistic conditions. These measurements also determined the rate constants of the cycloreversion reactions and assessed high selectivities to the respective oxa-NBDs.

Overall, the symmetric substitution of the parent NBD framework does not only enhance the absorption properties regarding the utilization of sun light but also influences the reactivity on the catalyst surface. Whereas the dibromo-substitution displayed partial dissociation upon adsorption on Ni(111), the derivatization with cyano moieties demonstrated a quantitative cycloreversion reaction of the QC derivative. The introduced oxa-NBD compounds yielded a completely switchable system on Pt(111) with a high thermal stability.

2.2.2. Asymmetric 2,3-Substitution of NBD/QC

The utilization of asymmetric substitution patterns is of advantage, as suitable substituents result in push-pull systems, featuring optimized electronic properties with higher bathochromic shifts of the absorption onset; still the molar mass can be kept reasonably low. The presented derivatives are sorted by their type of trigger for initiating the energy-releasing cycloreversion reaction: After discussing experiments with catalytic triggering, findings of electrochemical studies are summarized; finally, the anchoring of NBD molecules is addressed, as an approach towards the realization of energy release in form of electricity (see introduction).

The chemistry of the push-pull conjugated 2-carbethoxy-3-phenyl-NBD (**NBD 5**) has been of interest due to its promising properties for practical applications. The absorption onset of **NBD5** was determined at 359 nm. Its facile conversion proceeds quantitatively without need of any photosensitizer ($\Phi_{310\,nm} > 70\%$).[110] At the same time, **QC5** displays a remarkably high stability ($t_{1/2}$: 450 days at 25 °C) in comparison to similar derivatives, and maintains a high storage potential of 88.3 $kJ\,mol^{-1}$.[54] The reversible isomerization of **NBD5** was illustrated by the use of [Fe₃O₄-CoSalphen], a hybrid nanoparticle catalyst; for this system, an external magnetic field

enabled a simple separation.[54] Linked cobalt porphyrins marked the second generation of this catalyst type, and showed an 22.6-fold increased performance.[110] The photochemistry of **NBD5** has also been explored regarding its full reaction coordinate during isomerization by time-resolved techniques, stating its dependence on the charge-transfer character of the NBD molecule.[111]

In the following, we address the catalytically triggered energy release for the molecule pairs. Surface science experiments of **NBD5** and its **QC5** isomer were conducted on different single crystal surfaces. Synchrotron radiation-based XP spectra allowed for the clear distinction of both valence isomers at low temperatures (115 to 125 K) on Pt(111) and Ni(111).[112] Contrary to unsubstituted NBD, there were no signs of an agostic Pt-H interaction between the CH₂ bridgehead and the surface; therefore, a side-on adsorption of **NBD5** was excluded on Pt(111). In the case of Ni(111), both isomers were suggested to bind very differently: Whereas a binding of **NBD5** via the oxygen atoms of its ester moiety was proposed, the counterpart **QC5** interacted through its QC framework and the phenyl ring with the substrate. The thermal evolution was assessed in temperature-programmed experiments. On Pt(111), the energy-releasing cycloreversion occurred between 140 and 240 K, with no formation of side products. Thermal decomposition of **NBD5** set in above 300 K, yielding CO next to C−H residues (see Figure 7). In contrast, Ni(111) did not show catalytic activity for the back conversion to **NBD5**; instead, both **NBD5** and **QC5** displayed an early fragmentation at 160 to 180 K, yielding CO and carbonaceous species. Notably, for **NBD5** only 10% of a monolayer coverage remained on the surface above 300 K, indicative of the weak oxygen-bound adsorption motif of the energy-lean isomer. This pronounced desorption of the NBD derivative, without further reactivity on the surface, is crucial for the design of reversible MOST cycles within the scope of heterogeneous catalysis.

Since Au(111) acted as highly active catalyst material for the conversion of **QC7** (see below), the molecule pair **NBD5/QC5** was also characterized on a gold surface in a combined synchrotron radiation photoelectron spectroscopy (SRPES) and IRRAS study under UHV conditions, along with PEC-IRRAS in the liquid phase.[113] Indeed, the high catalytic activity of gold was also confirmed for **QC5**, as the contact with the catalyst led to the instantaneous cycloreversion reaction to **NBD5**, even at cryogenic temperatures of ~110 K; specifically, no spectroscopic differences were detectable upon adsorption of submonolayers of **NBD5** and **QC5**. Only for multilayer exposure, **QC5** was stable as frozen film. At higher temperatures, the increased mobility in the multilayer film led to the reaction to **NBD5**, when reaching the catalyst surface. Multilayer desorption occurred above 232 K, whereas residual **NBD5** at lower coverages desorbed shortly afterwards. The liquid-phase experiments verified the rapid cycloreversion of **QC5** by Au(111), with a similar half-life as for **QC7** (see below) and thus comparable rate constants. Due to a high selectivity of the reaction, there were no signs for degradation even after 100 energy storage and release cycles but in fact a slight increase in activity over time.
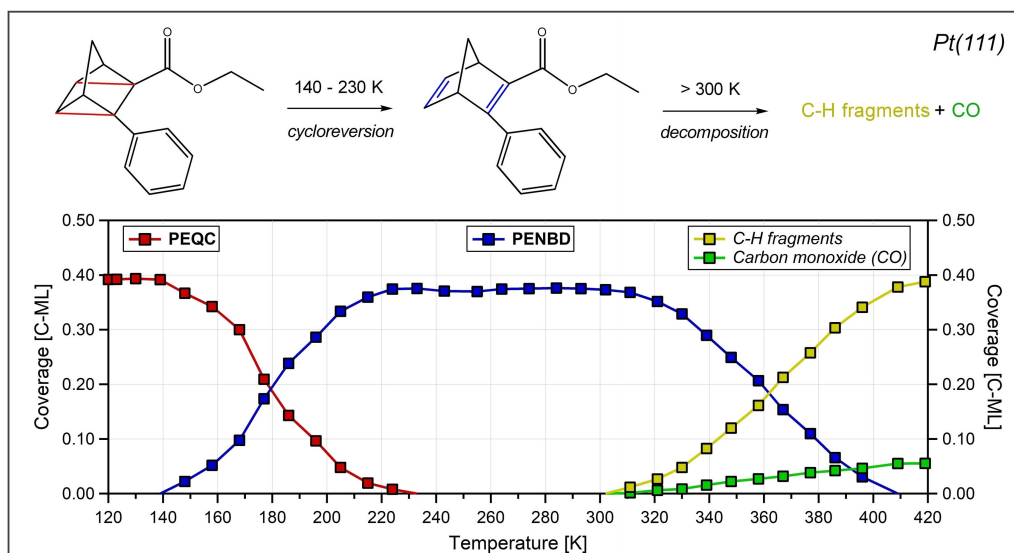
Figure 7. Proposed reaction pathway of PEQC (**QC5**) on Pt(111) as a result of the TPXPS experiment: between 140 and 230 K, monitoring of the quantitative cycloreversion reaction to PENBD (**NBD5**); above 300 K, decomposition into carbon monoxide (CO) and C—H fragments. Reprinted with permission from Ref. [112] under license CC BY 4.0 DEED. Copyright (2023) John Wiley and Sons.[112]

The cycloreversion can also be induced electrochemically by applying an external potential. The influence of the substitution on the triggered heat release of QC systems was assessed by Franz *et al.* in a comparative study of **QC5** with **QC6**; compared to **QC5**, the latter is extended by a methoxy group in *para*-position of the phenyl substituent.[114] DFT modelling gave insights into the respective energetic differences of the oxidative reaction channel. The stronger electron donating character of **QC6** resulted in a decreased ionization energy. Differential pulse voltammograms displayed a pronounced feature of **QC5** at 0.6 V_{fc}, as compared to a small signal at 0.45 V_{fc} for **QC6**. The latter one was associated with the formation of low amounts of **QC6$^{+\bullet}$** radicals that initiate a chain reaction (autocatalytic reaction) for the cycloreversion to **NBD6**; in contrast, the oxidation of **QC5** yielded decomposition products to some extent. After having determined spectroscopic markers for the respective derivatives, PEC-IRRAS measurements in acetonitrile (MeCN) on a HOPG crystal allowed for quantifying the back conversions, which were followed as a function of the applied potential. For **QC5**, a partial reaction to **NBD5** already set in between -0.9 and 0.3 V_{fc}, possibly caused by solvent effects or reactive species formed; a rapid cycloreversion was found for potentials higher than 0.5 V_{fc}. However, the selectivity for this derivative amounted only to 60%. **QC6** was stable at low potentials and a complete conversion to **NBD6** was electrochemically induced, starting at 0.3 V_{fc} and finished at 0.4 V_{fc}. A measured degradation of about 30% after 100 cycles stated its high selectivity (> 99.3%). Thus, the electrochemical stability of structurally very similar derivatives differed substantially, being, however, tunable by appropriate molecular design. The authors concluded that the observed charge-efficient energy release mechanism, with about 20 **NBD6** units converted per formed **QC6$^{+\bullet}$** radical through one electron, had an almost negligible effect on the total energy efficiency of the MOST system. In total, an estimate of 0.017 *kJ* heat was deduced for an input of 1 *C* electric charge.

As further MOST system, 2-cyano-3-(3,4-dimethoxyphenyl)-NBD (**NBD7**) and its corresponding QC isomer were tested as promising asymmetric cyano derivatives. Waidhas *et al.* investigated the electrochemically controlled cycloreversion reaction of **QC7** on a Pt(111) electrode in dichloromethane (DCM). They focused on the overall reversibility of the system by PEC-IRRAS, combined with DFT calculations for the assignment of characteristic bands.[115] Exhibiting a reasonable quantum yield ($\Phi_{340\ nm} = 68$%) of the photoconversion of **NBD7**, the energy-rich **QC7** was found to be stable on the electrode surface at a potential of -0.88 V_{fc}. The energy-releasing cycloreversion reaction was triggered between 0.02 and 0.92 V_{fc} with full selectivity, whereby at higher potentials the degradation of **NBD7** occurred; note that conversion of **QC7** to **NBD7** already set in partly below 0.02 V_{fc} due to the catalytic activity of platinum. From cyclic voltammetry measurements, no distinct oxidation of **QC7** was observed, which proved the autocatalytic reaction pathway of the cycloreversion. The reversibility of > 99% for each isomerization cycle was determined after 1000 conducted cycles. A pronounced decline in efficiency (50% after ~70 cycles) for the reconversion was attributed to electrode fouling over time, as also confirmed in an *ex situ* XPS analysis. This conclusion led to a follow-up study of the same molecule pair on the HOPG electrode.[116] After confirmation of a quantitative photoconversion of **NBD7** to **QC7**, this time, a broader stability range of **QC7** was observed between -0.88 to 0.02 V_{fc}. In contrast, on Pt(111), slow cycloreversion was already observed below 0.02 V_{fc}, as described above, due to a competing catalytic reaction channel. Utilizing HOPG, the reconversion was only triggered electrochemically, when reaching values above 0.02 V_{fc} and the formed **NDB7** had a stability limit at 0.82 V_{fc}. *In situ* PEC-IRRAS experiments provided

information on the cyclability of the system. The suppression of the catalytic activity of the electrode increased the reversibility to about 99.8 % per cycle, yielding a slower loss of storage capacity (50 % after ~400 cycles). Yet, minor decomposition was suggested due to radical-induced polymerization reactions.

Surface investigations of the same molecule system, **NBD7** and **QC7**, on Au(111) further emphasized the advantages of both heterogeneous catalysis and electrochemical control.[117] PEC-IRRAS experiments in MeCN showed the conversion to **QC7** upon irradiation, whereby the direct contact to the Au(111) surface effected a fast back reaction, giving a steady-state concentration. The catalytic activity was more than 200 times higher than for Pt(111), possibly due to less electrode poisoning. Having turned off the UV light, all **QC7** was rapidly converted to **NBD7**. A rate constant of 2×10^{-4} ms^{-1} was determined for the cycloreversion at open-circuit potential. The observed kinetics of the back conversion could be tuned by applying an external potential. Thereby, a change of the potential from -0.3 to -1.0 V$_{fc}$ impeded the conversion rate by a factor of 60. The authors described this behavior as "catalytic valve" for triggering the energy release. Moreover, constant-current-mode STM images of the Au(111) catalyst after irradiation of the used solvent and NBD system for 60 min gave no signs of holes or roughening, indicating the absence of surface corrosion or etching during operation; minor islands are due to residues of **NBD7** still adsorbed after rinsing (see Figure 8). Overall, no decomposition was detected even after 1000 storage cycles, while the activity was reduced by just 0.1 % per cycle.

Next, the anchoring of MOST molecules on the surface is discussed, which was achieved by suitable molecular platforms. As outlined in the introduction, the linkage to suitable electro-des allows for the favorable energy release as electricity (see Scheme 4). Schlimm et al. elucidated the surface catalysis of the cis-trans isomerization of anchored azobenzene derivatives on Au(111), which strongly enhanced the reaction rates for the energy release.[118] A tuning of the coupling with the surface was possible through molecular design based on triazatriangulenium (TATA) platforms, which formed well-defined surface structures but maintained their photoswitching capabilities on Au(111).[11e,119] Methodical investigations of the electronic coupling led to the conclusion that a mixing of molecular and gold states occurs, which enables an intersystem crossing between the singlet and triplet states in the relaxation process, mediated by the substrate.[118] Analogously, the first NBD-functionalized TATA molecular systems were considered; STM images of NBD-TATA molecules showed the adsorption of self-assembled monolayers on Au(111) with long-range order.[120] In addition, trioxatriangulenium (TOTA) was chosen as slightly modified and more stable mount for linked NBD frameworks. By attaching an asymmetric cyano NBD unit to the TOTA platform (**NBD8**), the corresponding energy-rich QC isomer (**QC8**) was found to be stable under ambient conditions, as no thermal back conversion took place.

The introduced NBD-TOTA derivative (**NBD8**) has been surveyed concerning its energy release on Au(111) by means of IRRAS.[121] The use of the TOTA platform enabled the formation of a well-ordered monolayer of **NBD8** on gold; the adsorption geometry was determined with the TOTA moiety parallel to the surface, while the cyano group is tilted and the NBD framework points towards vacuum. Moreover, the above-described mechanism of direct electronic coupling to gold was supposed to reduce the probability of side reactions and decomposition routes, achieving a higher reversibility of the storage cycle. DFT
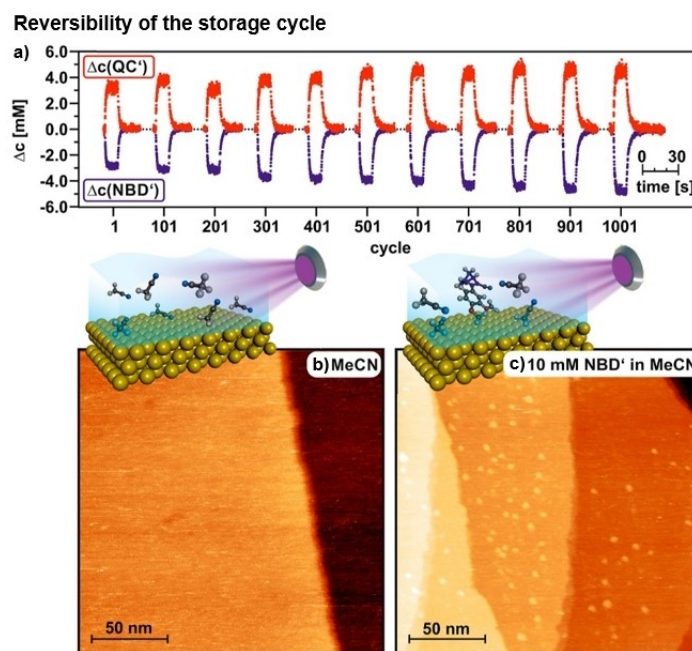
Figure 8. Reversibility test of the isomerization between NBD' (**NBD7**) and QC' (**QC7**) on Au(111) by PEC-IRRAS and STM. (a) Development of concentrations in the course of 1000 conducted energy storage and release cycles. Evaluation of Au(111) surface by STM (0.1 nA; 0.2 V) after irradiation at open-circuit potential for 60 min in (b) MeCN and (c) 10 mM NBD' (**NBD7**) in MeCN. Adapted with permission from Ref. [117]. Copyright (2022) American Chemical Society.[117]

ChemPhysChem

Review
doi.org/10.1002/cphc.202300806

**Chemistry
Europe**
European Chemical
Societies Publishing

calculations predicted an energy difference between the isomers of 0.8 to 1.2 eV, being comparable to non-functionalized NBD. Irradiation of **NBD8** at 310 nm yielded complete conversion to **QC8**, whereby the CN group acted as spectroscopic marker in the experiments, since the characteristic band displayed a detectable shift upon isomerization. An intact adsorption of **NBD8** was observed at 110 K, whereby disordered multilayers desorbed above 320 K. Due to strong van der Waals interactions of the TOTA unit, the remaining monolayer was stable up to 600 K. As anticipated by the high catalytic activity of Au(111), a photoinduced isomerization to **QC8** was not possible in the monolayer, which was attributed to the fast proceeding back conversion to **NBD8** on the timescale of the measurements. Only for coverages of at least two layers, the molecules that were not in contact with the catalyst surface were switched to the QC derivative (see Figure 9).

To obtain well-defined NBD films of high quality on a semiconducting oxide, Schwarz et al. surveyed the anchoring of carboxyl-functionalized NBD on an atomically ordered cobalt oxide surface by IRRAS.[122] Specifically, the adsorption of 1-(2′-norbornadienyl)pentanoic acid (**NBD9**) on $Co_3O_4(111)/Ir(100)$ was examined in isothermal experiments, and the subsequent thermal evolution was followed by temperature-programmed measurements. By comparison with a dataset of benzoic acid, **NBD9** was found to be deprotonated at 130 K and having formed a symmetric chelating carboxylate. For higher exposures, the observed multilayer did not show any preferential orientation and desorbed at 240 K. Deposition of **NBD9** at 300 K

gave only anchored molecules; upon increasing dosage, the initially flat-lying **NBD9** species oriented towards an upright-standing binding motif (see Figure 10d). The thermal stability of the thereby-prepared high coverage film was assured up to 400 K.

As first model system towards the release of the stored energy in electrical form, the photoswitching of 2-cyano-3-(4-carboxyphenyl)-NBD (**NBD10**), coupled to cobalt oxide as a semiconductor, was assessed by IRRAS.[50] The exposure of the $Co_3O_4(111)$ surface to **NBD10** led to the formation of a completely anchored monolayer, followed by the growth of a multilayer film. Upon heating, the desorption of the multilayers was found to occur at 280 K, with the monolayer being stable up to 570 K. The photochemical conversion to **QC10** was monitored quantitatively with the determination of the corresponding quantum efficiencies, showing a dependence on the film thickness and NBD concentration. The thermal activation barrier for the back conversion from **QC10** to **NBD10** is 103 $kJ\ mol^{-1}$, as determined from isothermal measurements between 350 and 370 K. Notably, anchoring the molecules on the surface did not affect this value. Overall, a high reversibility (98.5%) during charging and discharging within the closed isomerization cycle between **NBD10** and **QC10** was reported at the atomically defined organic-oxide hybrid interface. The same combination of derivative and surface was used in a subsequent study on the transition to the liquid phase and the electrochemical control therein by PEC-IRRAS.[123] The photoinduced isomerization to **QC10** was also feasible in solution (DCM): The
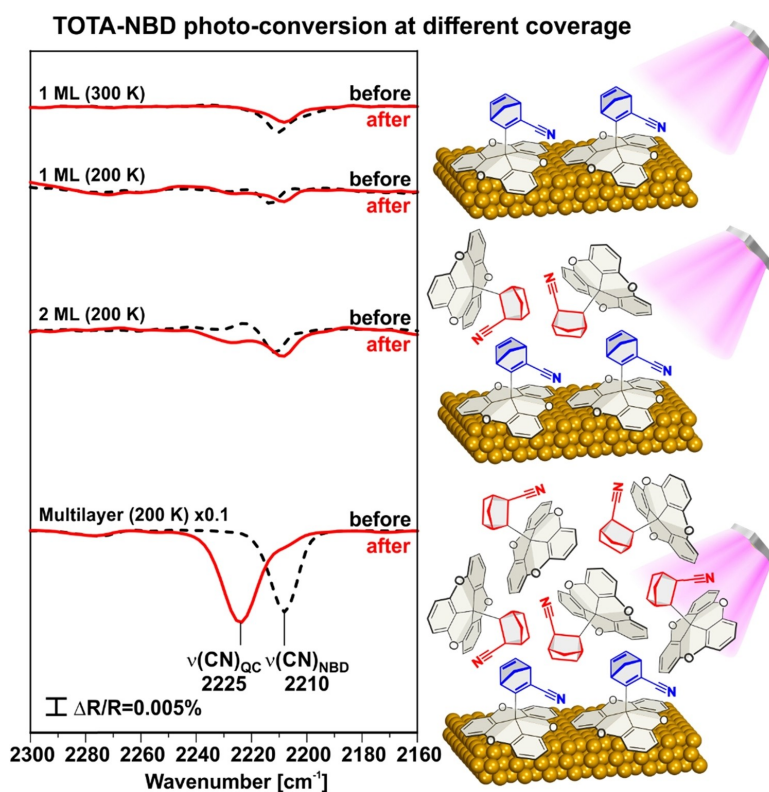
Figure 9. Comparison of IRRA spectra before and after irradiation of TOTA-NBD (**NBD8**) films at different coverages on Au(111). For an ordered monolayer, no formation of TOTA-QC (**QC8**) is observed due to the high catalytic activity of the gold surface, independent of the temperature. Only starting at the second layer, contributions by TOTA-QC (**QC8**) species are monitored. Reprinted with permission from Ref. [121]. Copyright (2022) Elsevier.[121]
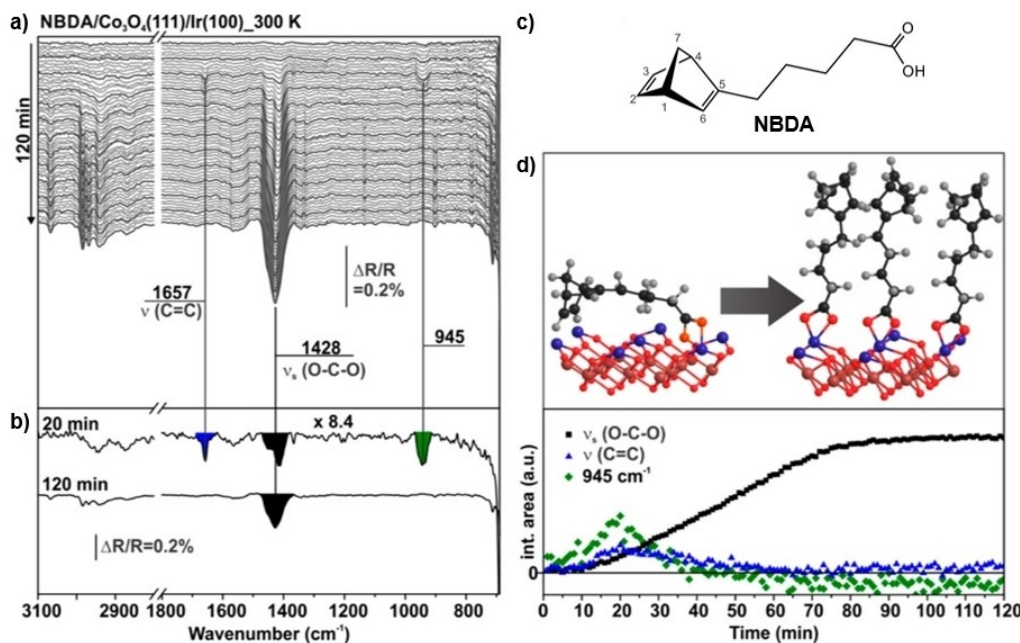
Figure 10. (a) Waterfall plot of IR spectra measured during adsorption experiment of NBDA (**NBD9**) on a Co$_3$O$_4$(111) film at 300 K. (b) Comparison between a submonolayer and saturated coverage. (c) Molecule structure of NBDA (**NBD9**). (d) Scheme of the deduced adsorption geometries with integrated contributions of characteristic bands at 1428, 1657, and 945 cm^{-1} as function of time. Adapted with permission from [122]. Copyright (2017) American Chemical Society.[122]

back reaction to **NBD10** was triggered with an onset potential of 0.1 V$_{fc}$, whereby 0.8 V$_{fc}$ marked the oxidative decomposition limit. To bridge the experiments to the previous investigations, an anchored monolayer was prepared under well-defined UHV conditions as model interface and was directly transferred into the liquid electrolyte, with no exposure to ambient conditions.[124] Both without and under potential control at −0.48 V$_{fc}$, the transfer yielded intact monolayer films of anchored **NBD10**, which were equally photoswitchable. However, the electrochemically triggered cycloreversion reaction of **QC10** was hindered since the required potential coincided with the irreversible oxidation of the photoswitch and thus its decomposition. Therefore, further molecular design studies of the surface-anchored molecules are necessary, which are resistant towards oxidative degradation at the potential needed for initiating the energy-releasing conversion from QC to NBD.

Altogether, it was illustrated that the versatile derivatization of NBD includes promising asymmetrically 2,3-substituted molecules. In comparison to a symmetrical substitution pattern (see Section 2.2.1), the introduction of push-pull systems causes an advantageous larger redshift of the absorption onset. Moreover, a facile and efficient photoconversion to the respective QC isomer is possible for most considered compounds. The presented surface science studies described different trigger for the energy release in the course of the cycloreversion reaction to the NBD derivative. Beside a catalytic reaction channel, electrochemical experiments revealed the practicality of a potential-induced back reaction. In particular, the substitution with ester or cyano moieties yields functional systems. The catalytic activity is dependent on the catalyst surface, whereby gold induced the highest energy release rates.

Finally, anchoring the molecules to the surface achieved high-quality films, whereby coupling to a suitable semiconductor is necessary for a future energy release in form of electricity.

3. Applications of Norbornadiene and Quadricyclane Derivatives

The technical applicability of NBD/QC as MOST system was already stated to be feasible in a process analysis of 1983, but the economic evaluation revealed no competitiveness back then, especially due to the low collector efficiency.[18a] For this reason, the implementation of NBD was limited to a use as additive or ligand, or in the field of synthetic applications, e.g., in polymer[125] and insecticide[126] production. For QC derivatives, a cytotoxic effect was described in combination with cisplatin as approach for the design of anticancer drugs.[127]

With respect to the application as energy storing unit, the intrinsic limitations of a low quantum yield of the photo-conversion and the small utilizable fraction of the incident solar energy have now been addressed by sophisticated molecular design. That is, compounds with similar or likewise derivatization as for the considered surface science investigations (see Table 1) were benchmarked. Please note the different reaction environments between the presented UHV studies and oper-ation conditions of actual NBD-based devices. Although not every potentially significant aspect can be included in these model catalytic experiments (pressure and material gap), the complexity of the systems is broken down by focusing on the adsorption and reaction behavior of the compounds. In this

ChemPhysChem

Review
doi.org/10.1002/cphc.202300806

Chemistry Europe
European Chemical
Societies Publishing

way, various molecule and catalyst combinations can be assessed in a well-defined manner. Identified trends are highly valuable to predict the performance for real-world applications. Further, the knowledge transfer from a fundamental mechanistic understanding enables the systematic optimization of MOST systems.

In particular, the syntheses of liquid MOST systems are of interest, as no addition of extra solvents is necessary for pumping. Dreos *et al.* introduced high-performing NBD derivatives that are functionalized with trifluoro methyl ketone and phenyl substituents.[53] These exhibited applicable viscosities at room temperature, high storage densities (up to 577 *kJ kg*$^{-1}$), and an absorption of up to 10% of the incoming solar light. The determination of quantum yields of an asymmetric cyano-NBD derivative was also carried out under conditions that are more realistic by irradiation of simulated sunlight, exhibiting high values and outstanding thermal stability; yet, intermolecular reactions caused minor photodegradation during cycling at higher concentrations.[128]

There are also many examples for the transition from laboratory demonstration to MOST devices. For some technical adaptions, the energy-storing molecules had to be embedded into processable matrices. Petersen *et al.* demonstrated the implementation of promising NBD derivatives into polystyrene, yielding a functional switching for day-to-day cycles; hereby, the application as energy storage coating, e.g., for window tinting[65] or as UV absorber[129] was suggested. Intrinsic and engineering limitations led to the development of hybrid solar technologies, wherein suitable MOST systems were combined with a solar water heating (SWH) system (see Figure 11). Thereby, both long storage and short term energy use was enabled at total efficiencies of up to 80% regarding the incoming sunlight, while maintaining a high stability with marginal degradation after more than 100 storage cycles.[130] Another hybrid concept involved the utilization of a phase-change material, separated by a silica aerogel from the NBD/QC storage unit. In this way, a potential 24/7 energy supply was proposed with high light harvesting (about 90% at large scale) at day and recover efficiencies of 80% at night.[131]

The release as heat is the most facile energy gained from MOST systems, which could be used for domestic heating and thermal power processes in industry. Already in 1988, a temperature increase of $> 50\,°C$ was realized in a fixed bed catalysis setup for unsubstituted QC[132] and first prototype derivatives.[133] The macroscopic heat release from more sophisticated molecules, fulfilling the most essential requirements for MOST applications, was tested by heterogeneous cobalt-based catalysts on a carbon support; a maximum temperature gradient of 63 °C was achieved for a 1.5 M solution at a measured temperature of 83 °C. The high reaction rate of $1.2\times10^4\,s^{-1}\,M^{-1}$ in toluene was in line with a low energetic barrier in complementary DFT calculations. An outdoor testing of the utilized system, with a ~900 cm^2 solar collector, demonstrated quantitative photoconversion and thus the feasibility under operation conditions.[134] In addition, the stored energy within MOST systems was also available as electricity by combination of the heat release of a QC derivative solution with microfabricated thermoelectric generator (MEMS-TEG) chips; power output densities of up to 1.3 W m^{-3} were measured.[18e]

Concluding, the efficiencies of test devices depend on the adjustment of the absorption behavior, molecular weight, storage time, energy barriers for the isomerization, and other
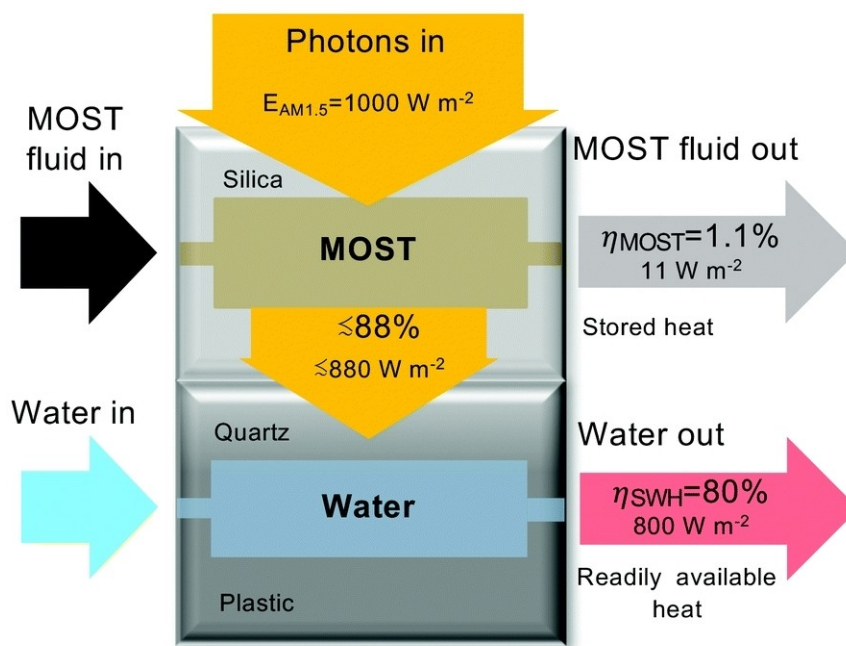

Figure 11. Composition of a microfluid hybrid device for solar energy conversion with MOST system as upper collector and a solar water heating unit underneath for transmitted photons with wavelengths larger than λ_{onset}. Reprinted with permission from Ref. [130] under license CC BY 3.0 DEED. Copyright (2017) Royal Society of Chemistry.[130]

physicochemical parameters. High storage densities of up to 250 $Wh\ kg^{-1}$, adaptable storage times (1 h to 18 years), and the overlap with the solar spectrum towards 590 nm were reached.[6e] Up-scaling of the syntheses of needed NBD derivatives was shown to be feasible by *in situ* cracking of dicyclopentadiene and the subsequent reaction with the respective acetylene derivate in a flow reactor.[135] Nonetheless, the general requirements for a practicality of MOST systems, as increased photoconversion yields, enhanced stabilities, and higher overall efficiencies, still present challenges that have to be subject of further investigations.

4. Summary and Outlook

In this review, we illustrated the evolution from the first discovery of the photoswitchable nature of norbornadiene as route for energy storage to the sophisticated molecular design of numerous derivatives with optimized properties. With simulated maximum efficiency limits of up to 21%,[136] the applicability of molecular solar thermal (MOST) systems appears promising in the context of novel energy storage materials. Next to thorough investigations on tuning the molecular characteristics in syntheses, the isomerization of the NBD derivatives to their respective energy-rich QC isomers has been studied extensively in the last decades. Nevertheless, profound information on the energy-release mechanism is necessary, as the fundamental understanding of the relevant reaction steps on the molecular level helps in the search for feasible systems. Concerning further applications, the general proof of concept was demonstrated in several laboratory-scaled test devices.

The specific focus of this review is on the surface chemistry of selected NBD derivatives on different heterogeneous model catalysts. Under well-controlled ultra-high-vacuum conditions and in liquid-phase experiments, mechanistic insights into the isomerization reactions between the NBD and QC molecules were gained. In particular, both the photoconversion to the strained QC upon irradiation and the cycloreversion to the relaxed NBD were analyzed with surface-sensitive techniques. It was shown that the energy release can be triggered in a thermal, catalytic, or electrochemical way. The selection of different catalyst materials was surveyed, and the type of catalytic reaction for the back conversion assessed, e.g., in a radical chain reaction or via a singlet-triplet mechanism. Moreover, the adsorption geometries of the MOST molecules on the surface were determined, or adjusted by using appropriate anchoring groups or platforms. The desorption behavior and thermal stability limits of the respective NBD systems were studied in temperature-programmed experiments, whereby entire surface reaction pathways were deduced with the aim of improved molecular design. The electrochemical characterization provided stability and reaction windows and indicated the potential-dependency of observed reaction rates. In addition, the reversibility of the isomerization reactions was monitored in several experiments giving a measure for the degradation over time.

In our opinion, the 2,3-disubsitution of NBD gives the ideal balance between optimized sun light absorbance and reasonable energy storage density. Next to established synthetic routes, the heterogeneously catalyzed energy release was found to be accessible. However, we learned that subtle structural changes of the molecules can profoundly affect their surface reactions and are difficult to predict. Also, the choice of catalyst has a major impact of the general feasibility and the reaction conditions. Besides, plenty new compound classes are not fully examined yet, so that, e.g., hetero-NBDs showed a great performance in first model experiments. The concept of an energy release in form of electricity is encouraging and would open completely new areas of application. That is, surface anchoring and coupling of the NBD derivatives to the substrate must be explored in more detail, ideally in multi-method surface science studies.

Despite the plethora of available NBD derivatives, the development of enhanced molecular features is still ongoing, supported by computational screening methods. In particular, the utilization of liquid MOST molecules seems to be advantageous, but also solid systems are applicable, e.g., in form of functional coatings. Prototype devices demonstrated increasing efficiencies over the last years. Yet, economic assessments also stress the importance of the number of life cycles of a system. In hybrid approaches, MOST units complement other modules by their unique light-harvesting and storage possibilities. Moreover, different individual requirements regarding absorption and storing properties can be satisfied by NBD-based devices. For that, surface science investigations are essential for a principle understanding and the non-arbitrary optimization of single parameters of a MOST system.

Conflict of Interests

The authors declare no conflict of interest.

[1] International Energy Agency, *World Energy Outlook 2022*, OECD Publishing, Paris, **2022**.

[2] a) M. Meinshausen, N. Meinshausen, W. Hare, S. C. Raper, K. Frieler, R. Knutti, D. J. Frame, M. R. Allen, *Nature* **2009**, *458*, 1158–1162; b) A. J. Weaver, K. Zickfeld, A. Montenegro, M. Eby, *Geophys. Res. Lett.* **2007**,

34, L19703; c) H. L. van Soest, M. G. J. den Elzen, D. P. van Vuuren, *Nat. Commun.* **2021**, *12*, 2140.

[3] a) D. Gielen, F. Boshell, D. Saygin, M. D. Bazilian, N. Wagner, R. Gorini, *Energy Strategy Rev.* **2019**, *24*, 38–50; b) C. Breyer, S. Khalili, D. Bogdanov, M. Ram, A. S. Oyewo, A. Aghahosseini, A. Gulagi, A. A. Solomon, D. Keiner, G. Lopez, P. A. Østergaard, H. Lund, B. V. Mathiesen, M. Z. Jacobson, M. Victoria, S. Teske, T. Pregger, V. Fthenakis, M. Raugei, H. Holttinen, U. Bardi, A. Hoekstra, B. K. Sovacool, *IEEE Access* **2022**, *10*, 78176–78218.

[4] Fraunhofer-Gesellschaft zur Förderung der angewandten Forschung e.V., Fraunhofer-Institut für Solare Energiesysteme ISE, in *Öffentliche Nettostromerzeugung in Deutschland im Jahr 2022* (Ed.: B. Burger), Freiburg, **2022**.

[5] C. Aoxia, P. K. Sen, in *IEEE Industry Applications Society Annual Meeting*, IEEE, Portland, OR, USA, **2016**, pp. 1–10.

[6] a) A. Lennartson, A. Roffey, K. Moth-Poulsen, *Tetrahedron Lett.* **2015**, *56*, 1457–1465; b) K. Moth-Poulsen, D. Ćoso, K. Börjesson, N. Vinokurov, S. K. Meier, A. Majumdar, K. P. C. Vollhardt, R. A. Segalman, *Energy Environ. Sci.* **2012**, *5*, 8534–8537; c) T. J. Kucharski, Y. C. Tian, S. Akbulatov, R. Boulatov, *Energy Environ. Sci.* **2011**, *4*, 4449–4472; d) Z. Wang, P. Erhart, T. Li, Z.-Y. Zhang, D. Sampedro, Z. Hu, H. A. Wegner, O. Brummel, J. Libuda, M. B. Nielsen, K. Moth-Poulsen, *Joule* **2021**, *5*, 3116–3136; e) J. Orrego-Hernández, A. Dreos, K. Moth-Poulsen, *Acc. Chem. Res.* **2020**, *53*, 1478–1487; f) Z. Wang, H. Hölzel, K. Moth-Poulsen, *Chem. Soc. Rev.* **2022**, *51*, 7313–7326.

[7] a) H.-D. Scharf, J. Fleischhauer, H. Leismann, I. Ressler, W. Schleker, R. Weitz, *Angew. Chem. Int. Ed.* **1979**, *18*, 652–662; b) G. Jones, S.-H. Chiang, P. T. Xuan, *J. Photochem.* **1979**, *10*, 1–18; c) Z.-i. Yoshida, *J. Photochem.* **1985**, *29*, 27–40.

[8] D. M. Gates, *Science* **1966**, *151*, 523–529.

[9] H. Bouas-Laurent, H. Dürr, *Pure Appl. Chem.* **2001**, *73*, 639–665.

[10] a) D. Schulte-Frohlinde, H. Blume, H. Güsten, *J. Phys. Chem.* **1962**, *66*, 2486–2491; b) C. Bastianelli, V. Caia, G. Cum, R. Gallo, V. Mancini, *J. Chem. Soc. Perkin Trans. 2* **1991**, *679–683*.

[11] a) H. Taoda, K. Hayakawa, K. Kawase, H. Yamakita, *J. Chem. Eng. Jpn.* **1987**, *20*, 265–270; b) A. R. Dias, M. E. Minas Da Piedade, J. A. Martinho Simões, J. A. Simoni, C. Teixeira, H. P. Diogo, Y. Meng-Yan, G. Pilcher, *J. Chem. Thermodyn.* **1992**, *24*, 439–447; c) H. M. Bandara, S. C. Burdette, *Chem. Soc. Rev.* **2012**, *41*, 1809–1825; d) Z. Wang, R. Losantos, D. Sampedro, M. Morikawa, K. Börjesson, N. Kimizuka, K. Moth-Poulsen, *J. Mater. Chem. A* **2019**, *7*, 15042–15047; e) S. Ulrich, U. Jung, T. Strunskus, C. Schutt, A. Bloedorn, S. Lemke, E. Ludwig, L. Kipp, F. Faupel, O. Magnussen, R. Herges, *Phys. Chem. Chem. Phys.* **2015**, *17*, 17053–17062; f) A. Goulet-Hanssens, M. Utecht, D. Mutruc, E. Titov, J. Schwarz, L. Grubert, D. Bleger, P. Saalfrank, S. Hecht, *J. Am. Chem. Soc.* **2017**, *139*, 335–341; g) E. Franz, A. Kunz, N. Oberhof, A. H. Heindl, M. Bertram, L. Fusek, N. Taccardi, P. Wasserscheid, A. Dreuw, H. A. Wegner, O. Brummel, J. Libuda, *ChemSusChem* **2022**, *15*, e202200958; h) E. Franz, J. Jung, A. Kunz, H. A. Wegner, O. Brummel, D. Mollenhauer, J. Libuda, *J. Phys. Chem. Lett.* **2023**, *14*, 1470–1477; i) K. Masutani, M. A. Morikawa, N. Kimizuka, *Chem. Commun.* **2014**, *50*, 15803–15806; j) C. Slavov, C. Yang, L. Schweighauser, C. Boumrifak, A. Dreuw, H. A. Wegner, J. Wachtveitl, *Phys. Chem. Chem. Phys.* **2016**, *18*, 14795–14804; k) A. M. Kolpak, J. C. Grossman, *Nano Lett.* **2011**, *11*, 3156–3162.

[12] a) H. Bouas-Laurent, J.-P. Desvergne, A. Castellan, R. Lapouyade, *Chem. Soc. Rev.* **2000**, *29*, 43–55; b) J. F. Xu, Y. Z. Chen, L. Z. Wu, C. H. Tung, Q. Z. Yang, *Org. Lett.* **2013**, *15*, 6148–6151.

[13] G. Jones, T. E. Reinhardt, W. R. Bergmark, *Sol. Energy* **1978**, *20*, 241–248.

[14] a) J. Daub, T. Knöchel, A. Mannschreck, *Angew. Chem. Int. Ed.* **1984**, *23*, 960–961; b) S. L. Broman, M. B. Nielsen, *Phys. Chem. Chem. Phys.* **2014**, *16*, 21172–21182; c) C. Schøttler, S. K. Vegge, M. Cacciarini, M. B. Nielsen, *ChemPhotoChem* **2022**, *6*, e202200037.

[15] a) G. Cottone, R. Noto, G. La Manna, *Chem. Phys. Lett.* **2004**, *388*, 218–222; b) M. Piantek, G. Schulze, M. Koch, K. J. Franke, F. Leyssner, A. Kruger, C. Navio, J. Miguel, M. Bernien, M. Wolf, W. Kuch, P. Tegeder, J. I. Pascual, *J. Am. Chem. Soc.* **2009**, *131*, 12729–12735.

[16] a) K. Börjesson, D. Ćoso, V. Gray, J. C. Grossman, J. Guan, C. B. Harris, N. Hertkorn, Z. Hou, Y. Kanai, D. Lee, J. P. Lomont, A. Majumdar, S. K. Meier, K. Moth-Poulsen, R. L. Myrabo, S. C. Nguyen, R. A. Segalman, V. Srinivasan, W. B. Tolman, N. Vinokurov, K. P. Vollhardt, T. W. Weidman, *Chem. Eur. J.* **2014**, *20*, 15587–15604; b) K. P. C. Vollhardt, T. W. Weidman, *J. Am. Chem. Soc.* **1983**, *105*, 1676–1677; c) Y. Kanai, V. Srinivasan, S. K. Meier, K. P. Vollhardt, J. C. Grossman, *Angew. Chem. Int. Ed.* **2010**, *49*, 8926–8929; d) R. Boese, J. K. Cammack, A. J. Matzger, K. Pflug, W. B. Tolman, K. P. C. Vollhardt, T. W. Weidman, *J. Am. Chem. Soc.* **1997**, *119*,

6757–6773; e) M. R. Harpham, S. C. Nguyen, Z. Hou, J. C. Grossman, C. B. Harris, M. W. Mara, A. B. Stickrath, Y. Kanai, A. M. Kolpak, D. Lee, D. J. Liu, J. P. Lomont, K. Moth-Poulsen, N. Vinokurov, L. X. Chen, K. P. Vollhardt, *Angew. Chem. Int. Ed.* **2012**, *51*, 7692–7696; f) A. Lennartson, A. Lundin, K. Börjesson, V. Gray, K. Moth-Poulsen, *Dalton Trans.* **2016**, *45*, 8740–8744.

[17] a) S. A. Brough, A. N. Lamm, S. Y. Liu, H. F. Bettinger, *Angew. Chem. Int. Ed.* **2012**, *51*, 10880–10883; b) J. Kim, J. Moon, J. S. Lim, *ChemPhysChem* **2015**, *16*, 1670–1675; c) K. Edel, X. Yang, J. S. A. Ishibashi, A. N. Lamm, C. Maichle-Mössmer, Z. X. Giustra, S. Y. Liu, H. F. Bettinger, *Angew. Chem. Int. Ed.* **2018**, *57*, 5296–5300.

[18] a) C. Philippopoulos, D. Economou, C. Economou, J. Marangozis, *Ind. Eng. Chem. Res.* **1983**, *22*, 627–633; b) V. A. Bren', A. D. Dubonosov, V. I. Minkin, V. A. Chernoivanov, *Russ. Chem. Rev.* **1991**, *60*, 451–469; c) A. D. Dubonosov, V. A. Bren, V. A. Chernoivanov, *Russ. Chem. Rev.* **2002**, *71*, 917–927; d) M. J. Kuisma, A. M. Lundin, K. Moth-Poulsen, P. Hyldgaard, P. Erhart, *J. Phys. Chem. C* **2016**, *120*, 3635–3645; e) Z. Wang, Z. Wu, Z. Hu, J. Orrego-Hernández, E. Mu, Z.-Y. Zhang, M. Jevric, Y. Liu, X. Fu, F. Wang, T. Li, K. Moth-Poulsen, *Cell Rep. Phys. Sci.* **2022**, *3*, 100789.

[19] O. Diels, K. Alder, *Liebigs Ann.* **1931**, *490*, 236–242.

[20] J. Hyman, Belgian Patent BE 498176, **1951**.

[21] a) J. Hine, J. A. Brown, L. H. Zalkow, W. E. Gardner, M. Hine, *J. Am. Chem. Soc.* **1954**, *77*, 594–598; b) A. F. Plate, M. A. Pryanishnikova, *Bull. Acad. Sci. USSR Div. Chem. Sci. (Engl. Transl.)* **1956**, *5*, 753–754.

[22] a) L. Schmerling, J. P. Luvisi, R. W. Welch, *J. Am. Chem. Soc.* **1956**, *78*, 2819–2821; b) S. J. Cristol, R. P. Arganbright, G. D. Brindell, R. M. Heitz, *J. Am. Chem. Soc.* **1957**, *79*, 6035–6039.

[23] a) L. Brjussowa, *Chem. Zentralbl.* **1936**, *107*, 2385–2386; b) M. Lipp, *Ber. Dtsch. Chem. Ges.* **1941**, *74*, 1–6; c) S. J. Cristol, *Tetrahedron* **1986**, *42*, 1617–1619.

[24] Y. Hirshberg, E. Fischer, *J. Chem. Soc.* **1953**, 629–636.

[25] a) S. J. Cristol, R. L. Snell, *J. Am. Chem. Soc.* **1954**, *76*, 5000; b) S. J. Cristol, R. L. Snell, *J. Am. Chem. Soc.* **1958**, *80*, 1950–1952.

[26] W. G. Dauben, R. L. Cargill, *Tetrahedron* **1961**, *15*, 197–201.

[27] G. S. Hammond, N. J. Turro, A. Fischer, *J. Am. Chem. Soc.* **1961**, *83*, 4674–4675.

[28] R. M. Moriarty, *J. Org. Chem.* **1963**, *28*, 2385–2387.

[29] a) C. D. Smith, *Org. Synth.* **1971**, *51*, 133–136; b) W. L. Dilling, *Chem. Rev.* **1966**, *66*, 373–393.

[30] N. J. Turro, W. R. Cherry, M. F. Mirbach, M. J. Mirbach, *J. Am. Chem. Soc.* **1977**, *99*, 7388–7390.

[31] J. Orrego-Hernández, H. Hölzel, Z. Wang, M. Quant, K. Moth-Poulsen, in *Molecular Photoswitches, Vol. 1* (Ed.: Z. L. Pianowski), Wiley-VCH, Weinheim, **2022**, pp. 350–378.

[32] a) X. W. An, Y. D. Xie, *Thermochim. Acta* **1993**, *220*, 17–25; b) D. S. Kabakoff, J. C. G. Buenzli, J. F. M. Oth, W. B. Hammond, J. A. Berson, *J. Am. Chem. Soc.* **1975**, *97*, 1510–1512.

[33] a) R. Hoffmann, R. B. Woodward, *J. Am. Chem. Soc.* **1965**, *87*, 2046–2048; b) R. B. Woodward, R. Hoffmann, *Angew. Chem. Int. Ed.* **1969**, *8*, 781–853.

[34] C. Qin, Z. Zhao, S. R. Davis, *J. Mol. Struct.* **2005**, *728*, 67–70.

[35] H. M. Frey, *J. Chem. Soc.* **1964**, 365–367.

[36] H. Hogeveen, H. C. Volger, *J. Am. Chem. Soc.* **1967**, *89*, 2486–2487.

[37] S. Miki, Y. Asako, Z.-i. Yoshida, *Chem. Lett.* **1987**, *16*, 195–198.

[38] a) G. S. Hammond, P. Wyatt, C. D. DeBoer, N. J. Turro, *J. Am. Chem. Soc.* **1964**, *86*, 2532–2533; b) T. Arai, T. Oguchi, T. Wakabayashi, M. Tsuchiya, Y. Nishimura, S. Oishi, H. Sakuragi, K. Tokumaru, *Bull. Chem. Soc. Jpn.* **1987**, *60*, 2937–2943.

[39] A. Cuppoletti, J. P. Dinnocenzo, J. L. Goodman, I. R. Gould, *J. Phys. Chem. A* **1999**, *103*, 11253–11256.

[40] a) S. Murov, G. S. Hammond, *J. Phys. Chem.* **1968**, *72*, 3797–3801; b) A. M. Helms, R. A. Caldwell, *J. Am. Chem. Soc.* **1995**, *117*, 358–361.

[41] a) K. Maruyama, K. Terada, Y. Yamamoto, *J. Org. Chem.* **1981**, *46*, 5294–5300; b) D. J. Fife, W. M. Moore, K. W. Morse, *J. Am. Chem. Soc.* **1985**, *107*, 7077–7083; c) D. P. Schwendiman, C. Kutal, *J. Am. Chem. Soc.* **1977**, *99*, 5677–5682; d) P. A. Grutsch, C. Kutal, *J. Am. Chem. Soc.* **1986**, *108*, 3108–3110.

[42] a) S. Lahiry, C. Haldar, *Sol. Energy* **1986**, *37*, 71–73; b) L. Pan, J.-J. Zou, X. Zhang, L. Wang, *Ind. Eng. Chem. Res.* **2010**, *49*, 8526–8531.

[43] Y. Harel, A. W. Adamson, C. Kutal, P. A. Grutsch, K. Yasufuku, *J. Phys. Chem.* **1987**, *91*, 901–904.

[44] M. Quant, A. Lennartson, A. Dreos, M. Kuisma, P. Erhart, K. Börjesson, K. Moth-Poulsen, *Chem. Eur. J.* **2016**, *22*, 13265–13274.

[45] M. Quant, A. Hamrin, A. Lennartson, P. Erhart, K. Moth-Poulsen, *J. Phys. Chem. C* **2019**, *123*, 7081–7087.

[46] G. Kaupp, H. Prinzbach, *Helv. Chim. Acta* **1969**, *52*, 956–966.

[47] A. Lennartson, M. Quant, K. Moth-Poulsen, *Synlett* **2015**, *26*, 1501–1504.

[48] M. Jevric, A. U. Petersen, M. Mansø, S. Kumar Singh, Z. Wang, A. Dreos, C. Sumby, M. B. Nielsen, K. Börjesson, P. Erhart, K. Moth-Poulsen, *Chem. Eur. J.* **2018**, *24*, 12767–12772.

[49] M. Mansø, A. U. Petersen, K. Moth-Poulsen, M. B. Nielsen, *Org. Biomol. Chem.* **2020**, *18*, 2113–2119.

[50] C. Schuschke, C. Hohner, M. Jevric, A. Ugleholdt Petersen, Z. Wang, M. Schwarz, M. Kettner, F. Waidhas, L. Fromm, C. J. Sumby, A. Görling, O. Brummel, K. Moth-Poulsen, J. Libuda, *Nat. Commun.* **2019**, *10*, 2384.

[51] M. Jevric, Z. Wang, A. U. Petersen, M. Mansø, C. J. Sumby, M. B. Nielsen, K. Moth-Poulsen, *Eur. J. Org. Chem.* **2019**, *2019*, 2354–2361.

[52] V. Gray, A. Lennartson, P. Ratanalert, K. Börjesson, K. Moth-Poulsen, *Chem. Commun.* **2014**, *50*, 5330–5332.

[53] A. Dreos, Z. Wang, J. Udmark, A. Ström, P. Erhart, K. Börjesson, M. B. Nielsen, K. Moth-Poulsen, *Adv. Energy Mater.* **2018**, *8*, 1703401.

[54] T. Luchs, P. Lorenz, A. Hirsch, *ChemPhotoChem* **2020**, *4*, 52–58.

[55] A. Padwa, M. J. Pulwer, R. J. Rosenthal, *J. Org. Chem.* **1984**, *49*, 856–862.

[56] K. J. Spivack, J. V. Walker, M. J. Sanford, B. R. Rupert, A. R. Ehle, J. M. Tocyloski, A. N. Jahn, L. M. Shaak, O. Obianyo, K. M. Usher, F. E. Goodson, *J. Org. Chem.* **2017**, *82*, 1301–1315.

[57] M. Mansø, L. Fernandez, Z. Wang, K. Moth-Poulsen, M. B. Nielsen, *Molecules* **2020**, *25*, 322.

[58] K. Jorner, A. Dreos, R. Emanuelsson, O. El Bakouri, I. Fdez. Galván, K. Börjesson, F. Feixas, R. Lindh, B. Zietz, K. Moth-Poulsen, H. Ottosson, *J. Mater. Chem. A* **2017**, *5*, 12369–12378.

[59] H. Prinzbach, *Pure Appl. Chem.* **1968**, *16*, 17–46.

[60] R. A. Valiulin, T. M. Arisco, A. G. Kutateladze, *J. Org. Chem.* **2013**, *78*, 2012–2025.

[61] H. Prinzbach, H. Bingmann, J. Markert, G. Fischer, L. Knothe, W. Eberbach, J. Brokatzky-Geiger, *Chem. Ber.* **1986**, *119*, 589–615.

[62] R. Meissner, X. Garcias, S. Mecozzi, J. Rebek, *J. Am. Chem. Soc.* **1997**, *119*, 77–85.

[63] H. J. Altenbach, H. D. Martin, B. Mayer, M. Müller, D. Constant, E. Vogel, *Chem. Ber.* **1991**, *124*, 791–801.

[64] M. Mansø, A. U. Petersen, Z. Wang, P. Erhart, M. B. Nielsen, K. Moth-Poulsen, *Nat. Commun.* **2018**, *9*, 1945.

[65] A. U. Petersen, A. I. Hofmann, M. Fillols, M. Mansø, M. Jevric, Z. Wang, C. J. Sumby, C. Müller, K. Moth-Poulsen, *Adv. Sci.* **2019**, *6*, 1900367.

[66] M. Mansø, B. E. Tebikachew, K. Moth-Poulsen, M. B. Nielsen, *Org. Biomol. Chem.* **2018**, *16*, 5585–5590.

[67] A. D. Dubonosov, S. V. Galichev, V. A. Chernoivanov, V. A. Bren, V. I. Minkin, *Russ. J. Org. Chem.* **2001**, *37*, 67–71.

[68] M. D. Kilde, M. Mansø, N. Ree, A. U. Petersen, K. Moth-Poulsen, K. V. Mikkelsen, M. B. Nielsen, *Org. Biomol. Chem.* **2019**, *17*, 7735–7746.

[69] E. Vessally, *J. Iran. Chem. Soc.* **2009**, *6*, 99–103.

[70] P. Lainé, V. Marvaud, A. Gourdon, J.-P. Launay, R. Argazzi, C.-A. Bignozzi, *Inorg. Chem.* **1996**, *35*, 711–714.

[71] M. Kuisma, A. Lundin, K. Moth-Poulsen, P. Hyldgaard, P. Erhart, *ChemSusChem* **2016**, *9*, 1786–1794.

[72] M. Nucci, M. Marazzi, L. M. Frutos, *ACS Sustainable Chem. Eng.* **2019**, *7*, 19496–19504.

[73] J. L. Elholm, A. E. Hillers-Bendtsen, H. Hölzel, K. Moth-Poulsen, K. V. Mikkelsen, *Phys. Chem. Chem. Phys.* **2022**, *24*, 28956–28964.

[74] N. Ree, M. Koerstz, K. V. Mikkelsen, J. H. Jensen, *J. Chem. Phys.* **2021**, *155*, 184105.

[75] U. Jacovella, E. Carrascosa, J. T. Buntine, N. Ree, K. V. Mikkelsen, M. Jevric, K. Moth-Poulsen, E. J. Bieske, *J. Phys. Chem. Lett.* **2020**, *11*, 6045–6050.

[76] R. B. King, S. Ikai, *Inorg. Chem.* **1979**, *18*, 949–954.

[77] K. C. Bishop, *Chem. Rev.* **1976**, *76*, 461–486.

[78] J. Manassen, *J. Catal.* **1970**, *18*, 38–45.

[79] M. J. Chen, H. M. Feder, *Inorg. Chem.* **1979**, *18*, 1864–1869.

[80] F. D. Mango, J. H. Schachtschneider, *J. Am. Chem. Soc.* **1967**, *89*, 2484–2486.

[81] L. Cassar, J. Halpern, *Chem. Commun.* **1970**, 1082–1083.

[82] G. F. Koser, P. R. Pappas, S.-M. Yu, *Tetrahedron Lett.* **1973**, *14*, 4943–4946.

[83] G. F. Koser, J. N. Faircloth, *J. Org. Chem.* **1976**, *41*, 583–585.

[84] P. G. Gassman, R. Yamaguchi, G. F. Koser, *J. Org. Chem.* **1978**, *43*, 4392–4393.

[85] a) J. L. Gébicki, J. Gébicki, J. Mayer, *J. Radiat. Phys. Chem.* **1987**, *30*, 165–167; b) E. Haselbach, T. Bally, Z. Lanyiova, P. Baertschi, *Helv. Chim. Acta* **1979**, *62*, 583–592.

[86] K. Yasufuku, K. Takahashi, C. Kutal, *Tetrahedron Lett.* **1984**, *25*, 4893–4896.

[87] P. G. Gassman, J. W. Hershberger, *J. Org. Chem.* **1987**, *52*, 1337–1339.

[88] O. Brummel, D. Besold, T. Döpper, Y. Wu, S. Bochmann, F. Lazzari, F. Waidhas, U. Bauer, P. Bachmann, C. Papp, H.-P. Steinrück, J. Libuda, J. Bachmann, *ChemSusChem* **2016**, *9*, 1424–1432.

[89] G. Ertl, *Angew. Chem. Int. Ed.* **2008**, *47*, 3524–3535.

[90] E. L. Muetterties, *Pure Appl. Chem.* **1982**, *54*, 83–96.

[91] M. C. Tsai, J. Stein, C. M. Friend, E. L. Muetterties, *J. Am. Chem. Soc.* **1982**, *104*, 3533–3534.

[92] M. J. Hostetler, R. G. Nuzzo, G. S. Girolami, L. H. Dubois, *Organometallics* **1995**, *14*, 3377–3384.

[93] M. Schwell, F. Dulieu, C. Gée, H.-W. Jochims, J.-L. Chotin, H. Baumgärtel, S. Leach, *Chem. Phys.* **2000**, *260*, 261–279.

[94] U. Bauer, S. Mohr, T. Döpper, P. Bachmann, F. Späth, F. Düll, M. Schwarz, O. Brummel, L. Fromm, U. Pinkert, A. Görling, A. Hirsch, J. Bachmann, H.-P. Steinrück, J. Libuda, C. Papp, *Chem. Eur. J.* **2017**, *23*, 1613–1622.

[95] O. Brummel, F. Waidhas, U. Bauer, Y. Wu, S. Bochmann, H.-P. Steinrück, C. Papp, J. Libuda, *J. Phys. Chem. Lett.* **2017**, *8*, 2819–2825.

[96] M. Schwarz, C. Schuschke, T. N. Silva, S. Mohr, F. Waidhas, O. Brummel, J. Libuda, *Rev. Sci. Instrum.* **2019**, *90*, 024105.

[97] U. Bauer, L. Fromm, C. Weiß, P. Bachmann, F. Späth, F. Düll, J. Steinhauer, W. Hieringer, A. Görling, A. Hirsch, H.-P. Steinrück, C. Papp, *J. Phys. Chem. C* **2019**, *123*, 7654–7664.

[98] R. L. Sams, T. A. Blake, *J. Mol. Spectrosc.* **2020**, *373*, 111354.

[99] M. H. Palmer, M. Coreno, M. de Simone, C. Grazioli, R. A. Aitken, S. V. Hoffmann, N. C. Jones, C. Peureux, *J. Chem. Phys.* **2020**, *153*, 204303.

[100] M. H. Palmer, S. V. Hoffmann, N. C. Jones, M. Coreno, M. de Simone, C. Grazioli, R. A. Aitken, *J. Chem. Phys.* **2021**, *155*, 034308.

[101] M. H. Palmer, S. V. Hoffmann, N. C. Jones, M. Coreno, M. de Simone, C. Grazioli, R. A. Aitken, C. Peureux, *J. Chem. Phys.* **2023**, *158*, 234303.

[102] F. Coppola, M. Nucci, M. Marazzi, D. Rocca, M. Pastore, *ChemPhotoChem* **2023**, *7*, e202200214.

[103] F. J. Hernández, J. M. Cox, J. Li, R. Crespo-Otero, S. A. Lopez, *J. Org. Chem.* **2023**, *88*, 5311–5320.

[104] S. Reinwardt, I. Baev, F. Linß, P. Cieslik, O. Raberg, T. Buhr, A. Perry-Sassmannshausen, S. Schippers, A. Müller, F. Trinter, A. Guda, R. Laasch, M. Martins, *Rev. Sci. Instrum.* **2023**, *94*, 023201.

[105] E. Vessally, *Russ. J. Phys. Chem. A* **2009**, *83*, 809–812.

[106] U. Bauer, L. Fromm, C. Weiß, F. Späth, P. Bachmann, F. Düll, J. Steinhauer, S. Matysik, A. Pominov, A. Görling, A. Hirsch, H.-P. Steinrück, C. Papp, *J. Chem. Phys.* **2019**, *150*, 184706.

[107] F. Hemauer, U. Bauer, L. Fromm, C. Weiß, A. Leng, P. Bachmann, F. Düll, J. Steinhauer, V. Schwaab, R. Grzonka, A. Hirsch, A. Görling, H.-P. Steinrück, C. Papp, *ChemPhysChem* **2022**, *23*, e202200199.

[108] M. A. Martin-Drumel, J. T. Spaniol, H. Hölzel, M. Agúndez, J. Cernicharo, K. Moth-Poulsen, U. Jacovella, *Faraday Discuss.* **2023**, *245*, 284–297.

[109] F. Hemauer, D. Krappmann, V. Schwaab, Z. Hussain, E. M. Freiberger, N. J. Waleska-Wellnhofer, E. Franz, F. Hampel, O. Brummel, J. Libuda, A. Hirsch, H.-P. Steinrück, C. Papp, *J. Chem. Phys.* **2023**, *159*, 074703.

[110] P. Lorenz, T. Luchs, A. Hirsch, *Chem. Eur. J.* **2021**, *27*, 4993–5002.

[111] W. Alex, P. Lorenz, C. Henkel, T. Clark, A. Hirsch, D. M. Guldi, *J. Am. Chem. Soc.* **2022**, *144*, 153–162.

[112] F. Hemauer, V. Schwaab, E. M. Freiberger, N. J. Waleska, A. Leng, C. Weiß, J. Steinhauer, F. Düll, P. Bachmann, A. Hirsch, H.-P. Steinrück, C. Papp, *Chem. Eur. J.* **2023**, *29*, e202203759.

[113] R. Eschenbacher, F. Hemauer, E. Franz, A. Leng, V. Schwaab, N. J. Waleska-Wellnhofer, E. M. Freiberger, L. Fromm, T. Xu, A. Görling, A. Hirsch, H.-P. Steinrück, C. Papp, O. Brummel, J. Libuda, *ChemPhotoChem* **2024**, *8*, e202300155.

[114] E. Franz, D. Krappmann, L. Fromm, T. Luchs, A. Görling, A. Hirsch, O. Brummel, J. Libuda, *ChemSusChem* **2022**, *15*, e202201483.

[115] F. Waidhas, M. Jevric, L. Fromm, M. Bertram, A. Görling, K. Moth-Poulsen, O. Brummel, J. Libuda, *Nano Energy* **2019**, *63*, 103872.

[116] F. Waidhas, M. Jevric, M. Bosch, T. Yang, E. Franz, Z. Liu, J. Bachmann, K. Moth-Poulsen, O. Brummel, J. Libuda, *J. Mater. Chem. A* **2020**, *8*, 15658–15664.

[117] E. Franz, C. Stumm, F. Waidhas, M. Bertram, M. Jevric, J. Orrego-Hernández, H. Hölzel, K. Moth-Poulsen, O. Brummel, J. Libuda, *ACS Catal.* **2022**, *12*, 13418–13425.

[118] A. Schlimm, R. Löw, T. Rusch, F. Röhricht, T. Strunskus, T. Tellkamp, F. Sönnichsen, U. Manthe, O. Magnussen, F. Tuczek, R. Herges, *Angew. Chem. Int. Ed.* **2019**, *58*, 6574–6578.

ChemPhysChem

Review
doi.org/10.1002/cphc.202300806

Chemistry Europe
European Chemical
Societies Publishing

[119] H. Jacob, S. Ulrich, U. Jung, S. Lemke, T. Rusch, C. Schutt, F. Petersen, T. Strunskus, O. Magnussen, R. Herges, F. Tuczek, *Phys. Chem. Chem. Phys.* **2014**, *16*, 22643–22650.

[120] R. Löw, T. Rusch, T. Moje, F. Rohricht, O. M. Magnussen, R. Herges, *Beilstein J. Org. Chem.* **2019**, *15*, 1815–1821.

[121] R. Eschenbacher, T. Xu, E. Franz, R. Löw, T. Moje, L. Fromm, A. Görling, O. Brummel, R. Herges, J. Libuda, *Nano Energy* **2022**, *95*, 107007.

[122] M. Schwarz, S. Mohr, T. Xu, T. Döpper, C. Weiß, K. Civale, A. Hirsch, A. Görling, J. Libuda, *J. Phys. Chem. C* **2017**, *121*, 11508–11518.

[123] M. Bertram, F. Waidhas, M. Jevric, L. Fromm, C. Schuschke, M. Kastenmeier, A. Görling, K. Moth-Poulsen, O. Brummel, J. Libuda, *J. Chem. Phys.* **2020**, *152*, 044708.

[124] F. Faisal, M. Bertram, C. Stumm, F. Waidhas, O. Brummel, J. Libuda, *Rev. Sci. Instrum.* **2018**, *89*, 114101.

[125] A. H. St. Amant, E. H. Discekici, S. J. Bailey, M. S. Zayas, J.-A. Song, S. L. Shankel, S. N. Nguyen, M. W. Bates, A. Anastasaki, C. J. Hawker, J. Read de Alaniz, *J. Am. Chem. Soc.* **2019**, *141*, 13619–13624.

[126] A. P. Marchand, B. Ganguly, C. I. Malagón, H. Lai, W. H. Watson, *Tetrahedron* **2003**, *59*, 1763–1771.

[127] U. M. Dzhemilev, A. R. Akhmetov, A. A. Khuzin, V. A. D'yakonov, L. U. Dzhemileva, M. M. Yunusbaeva, L. M. Khalilov, A. R. Tuktarov, *Russ. Chem. Bull.* **2019**, *68*, 1036–1040.

[128] A. Kjaersgaard, H. Hölzel, K. Moth-Poulsen, M. B. Nielsen, *J. Phys. Chem. A* **2022**, *126*, 6849–6857.

[129] Z. Refaa, A. Hofmann, M. F. Castro, J. O. Hernandez, Z. Wang, H. Hölzel, J. W. Andreasen, K. Moth-Poulsen, A. S. Kalagasidis, *Appl. Energy* **2022**, *310*, 118541.

[130] A. Dreos, K. Börjesson, Z. Wang, A. Roffey, Z. Norwood, D. Kushnir, K. Moth-Poulsen, *Energy Environ. Sci.* **2017**, *10*, 728–734.

[131] V. Kashyap, S. Sakunkaewkasem, P. Jafari, M. Nazari, B. Eslami, S. Nazifi, P. Irajizad, M. D. Marquez, T. R. Lee, H. Ghasemi, *Joule* **2019**, *3*, 3100–3111.

[132] S. Miki, Y. Asako, M. Morimoto, T. Ohno, Z.-i. Yoshida, T. Maruyama, M. Fukuoka, T. Takada, *Bull. Chem. Soc. Jpn.* **1988**, *61*, 973–981.

[133] S. Miki, T. Maruyama, T. Ohno, T. Tohma, S.-i. Toyama, Z.-i. Yoshida, *Chem. Lett.* **1988**, *17*, 861–864.

[134] Z. Wang, A. Roffey, R. Losantos, A. Lennartson, M. Jevric, A. U. Petersen, M. Quant, A. Dreos, X. Wen, D. Sampedro, K. Börjesson, K. Moth-Poulsen, *Energy Environ. Sci.* **2019**, *12*, 187–193.

[135] J. Orrego-Hernández, H. Hölzel, M. Quant, Z. Wang, K. Moth-Poulsen, *Eur. J. Org. Chem.* **2021**, *2021*, 5337–5342.

[136] Z. Wang, H. Moïse, M. Cacciarini, M. B. Nielsen, M. A. Morikawa, N. Kimizuka, K. Moth-Poulsen, *Adv. Sci.* **2021**, *8*, 2103060.